

A shift in time: time-lapse detection using interferometry

David C. Henley

ABSTRACT

Most seismic time-lapse studies examine the differences between a ‘baseline’ seismic image and a ‘time-lapse’ image, both obtained using the same acquisition parameters and seismic processing stream. The goal is to find a residual amplitude anomaly which can be associated with a change in the reflectivity of a boundary between two formations, where one of the formations has had its properties changed by fluid injection or extraction. Often, the amplitude anomaly is relatively small and difficult to detect. In this case, a secondary effect may prove to be more easily observed; the changed seismic transit time through the affected layer may cause a detectable time delay (or advance) of all reflections from layers beneath the target formation. We demonstrate here a method designed to detect very small time shifts, of less than one sample interval, between comparable portions of seismic images whose contributing data were recorded and processed with identical parameters. We first demonstrate the feasibility of detection with a simple image simulation; then we adapt the near-surface correction technique known as raypath interferometry to implement this difference technique. Results are first shown for a numerical model, then for a field survey for which previous anomaly analysis, based mainly on reflection amplitudes, has always been ambiguous.

INTRODUCTION

The detection of small differences between seismic images of the same subsurface region is of considerable interest, since ‘time-lapse’ surveys are being increasingly used not only to monitor the ongoing production of hydrocarbons, but also the sequestration of CO₂ in subsurface formations. The fluid content of porous rocks influences various rock property parameters, particularly wave propagation velocities and elastic moduli; hence changes of fluids within the rocks alter the rock properties, causing changes of reflectivity between layers, and wave propagation transit time through them. Comparing seismic images of the same rocks before and after changes in fluid content can highlight these differences and show their subsurface location. Most time-lapse surveys focus on detecting the difference in reflectivity between the target formation and the formations immediately above or below, since this is manifested as an amplitude ‘anomaly’ in the difference image formed by subtracting the two images. This is usually considered the most direct and useful diagnostic for time-lapse studies, since often the lateral extent of the image anomaly gives a direct indication of the actual subsurface extent of the fluid injection or withdrawal in the target formation. There are circumstances, however, when the reflection anomaly cannot be reliably detected; in these cases, it may be possible, instead, to analyze the small changes in transit time of waves passing through the affected formation and reflecting from deeper layer boundaries.

Detecting small time shifts

The detection of small time shifts between corresponding events on two seismic images might seem to be counterintuitive, since we usually consider vertical event resolution in terms of the conventional criterion of a layer thickness needing to be at least

$\frac{1}{4}$ wavelength of the predominant seismic frequency in order for the layer to be reliably detected. From rock property calculations for particular time-lapse surveys, on the other hand, we find that transit time differences through target layers due to fluid injection can often be as small as a fraction of a seismic sample interval (Zhang et al, 2005, Liu et al, 2005). How can such small time delays be detected when we can't even typically resolve the thin layer which causes them? As we will show later in a simulation, when the event amplitudes are properly normalized, a simple subtraction will readily detect very small time shifts between different images of the same event, even in the presence of significant noise. In other words, the same subtraction process usually used to highlight amplitude differences in an injection zone can, *with proper care*, be used to highlight instead the transit time differences caused by the same injection process. In this case, the 'proper care' consists of ensuring that the two images are precisely aligned in transit time (to within a fraction of a sample interval) before subtraction, a process made difficult by the necessity of applying independent, seasonally-varying near-surface weathering corrections to two vintages of seismic data. Henley et al (2012, 2016) illustrated the difficulty of doing this in a time-lapse model study; this is why most time-lapse studies focus on the generally easier objective of looking for reflection amplitude differences.

Henley et al (2012, 2016) showed that a major difficulty with time-difference diagnostics is the process of detecting and applying weathering corrections, which must be independent for each vintage of seismic data, since the acquisition conditions inevitably differ for two surveys performed at significant time intervals. Since weathering corrections for most surveys typically range over a few tens of milliseconds, and we hope to detect event time differences of fractions of a millisecond, some process must be found to reconcile the weathering corrections, or to bypass them entirely. During our 2012 model study, we found, serendipitously, that using an interferometric process for finding and applying weathering corrections allowed two surveys to be aligned precisely enough that very small transit time anomalies became readily visible, even when the amplitude anomaly was not as easily detectable. Below, we give a brief explanation.

Conventional weathering corrections (statics)

Since time-lapse seismic studies seek to detect what can be quite small differences in subsurface conditions, most of the difficulties in time-lapse detection are associated with ensuring that seismic surveys to be compared are as similar as possible in all their acquisition and processing parameters. Even when acquisition geometry and processing flows are repeated exactly for two surveys, however, the issue most likely to affect the detectability of a time-lapse anomaly is that of correcting the two vintages of seismic data for the effects of the surface weathered layer, whose properties can change considerably over the duration of a time-lapse experiment, due to seasonal and weather-related conditions, like soil moisture content and surface temperature (frozen surface in winter). The most common corrections applied to seismic data are time shifts of the raw input traces, where the shifts are computed and applied based on the principle of aligning reflection events to provide the greatest "power" or amplitude when stacked or summed over common midpoint coordinates. The commonly-used maximum-stack-power residual statics programs are relatively successful in finding and applying individual trace shifts that maximize reflection event coherence and amplitude; but for two different vintages of the same reflections, small time differences in the overall images, particularly long-

wavelength lateral variations, and often a small bulk shift, can result between independent applications of the autostatics program to the two vintages of seismic data (we cannot simply use the same statics solution for both images, since the actual weathering corrections will inevitably be different for the two data vintages). If the statics solutions are good ones, the differences between baseline and time-lapse images may be quite small, and this may not significantly affect *reflection amplitude differences* between events on the images; but it can mask the ability to detect very small *transit time anomalies* between specific events on the two images.

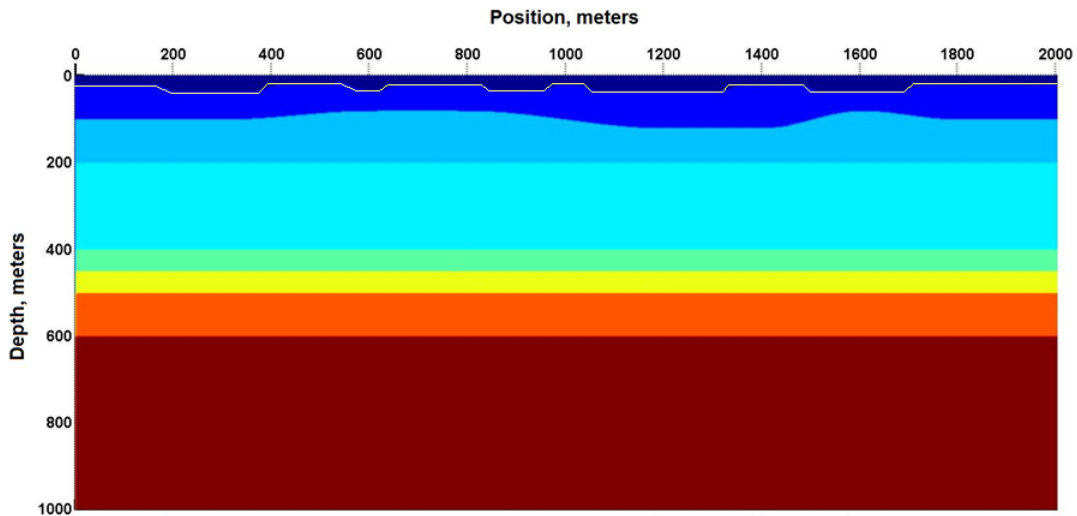
Raypath interferometry

A recently-developed technique called raypath interferometry (Henley 2012a, 2012b, Cova et al 2015) can also be used to remove the near-surface weathering effects from seismic reflection data; and it can be applied in a way which guarantees no bulk shifts or long-wavelength structural differences between two images of the same reflection sequence. The reason for this lies in the basic difference between this method and conventional maximum-stack-power autostatics. Whereas autostatics programs are designed to detect and remove *vertical-incidence* time shifts to maximize the stack power of *all events* within a correlation window on CMP ensembles, the raypath interferometry method detects and removes *raypath-dependent* ‘surface functions’. If we use the same ‘reference wavefield’ to apply raypath interferometry to two different images, we ensure that corrections applied while creating the images will produce no net shift between them. Furthermore, since raypath interferometry is *non-stationary*, the corrections applied to shallow data on each survey are independent of those applied to deeper data. This means that ‘time sag’ evidenced on deeper events in the time lapse survey will be properly preserved and not affected by corrections applied to shallower events.

Evidence

We were first led to investigate interferometric weathering corrections for time-lapse studies by the results of a finite difference numerical model study performed in 2012 (Henley et al, 2012, Henley et al, 2016). In this study, we investigated various acquisition and processing issues affecting the detectability of a relatively large and shallow time-lapse anomaly placed in a model with mild near-surface structure, as well as significant weathering anomalies at the surface. Figure 1 is a schematic of both the baseline model (Figure 1a) and the time-lapse model (Figure 1b), while Figure 2 shows a typical source gather without (Figure 2a), and with (Figure 2b) the complications (statics, scattered linear noise) caused by the near-surface weathering anomalies. The raw finite-difference source gathers for both the baseline and time-lapse models in Figure 1 resembled that in Figure 2b, except with the addition of a significant level of random noise. Prior to processing, the data set for the time-lapse model was further modified by creating two sets of uncorrelated random static shifts and applying one set to all the raw traces by common source station number, then applying the other set to the raw traces by common receiver station number. These static shifts simulated the ‘seasonal variations’ in the surface-consistent statics expected for surveys acquired at significantly different times.

Baseline Model



b) Monitor Model

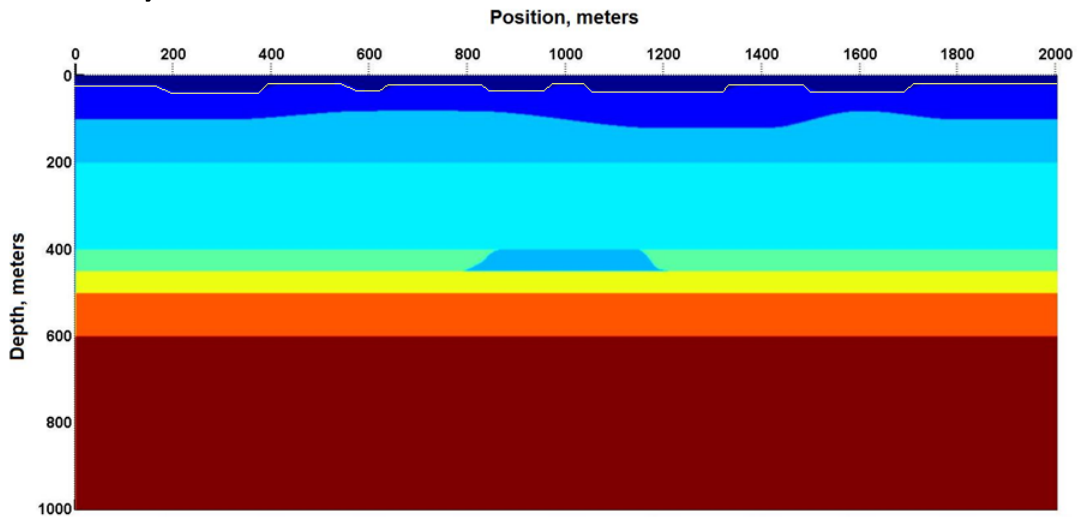


FIG. 1. a) Baseline model, with near-surface structure and surface irregularities, which lead to scattering and event time delays. b) Same as baseline model, except for an anomalous zone simulating fluid injection at 400m depth.

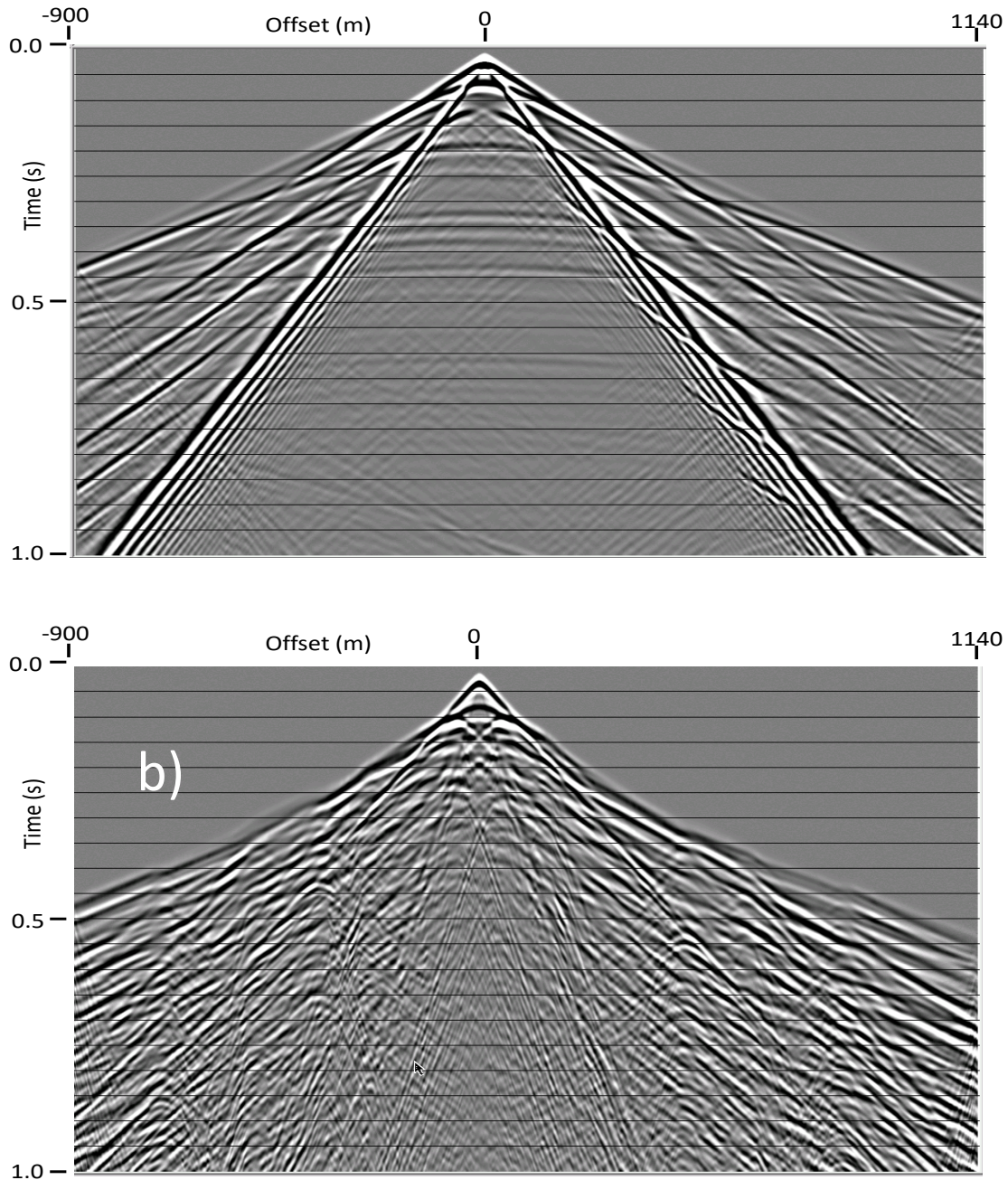


FIG. 2. a) Typical finite difference elastic source gather for the Baseline model in Figure 1a, but without the surface irregularities. b) Typical source gather for the Baseline model in Figure 1a, including the scattering and time delays caused by the surface irregularities. Random noise (RMS S/N = 1.0) was later added to all source gathers for both Baseline and Monitor models.

The data sets for both baseline and time-lapse surveys were processed using the same processing stream and the same parameters. In each case, the data were initially subjected to radial-trace coherent noise attenuation to remove direct arrivals, ground roll, and scattered source arrivals. Gabor deconvolution was then applied to whiten the data. A maximum-stack-power autostatics program was used to provide surface-consistent statics

solutions for each data set independently. Because of the strength of the additive random noise, three passes of autostatics were needed in each case. Following autostatics, NMO was removed from each data set, and a CMP stack image created. Figures 3 and 4 show the resulting images; it is difficult to see the time-lapse anomaly until the images are subtracted, as in Figure 5. *It should be noted that in order to create this difference image, the baseline survey image was shifted by 6ms (trial and error) in order to properly align the reflections and minimize their differences.* This is due to the difference between the means of the autostatics solutions involved in creating the two images. The fragmentary events along the top of the difference image (Figure 5) essentially show the effect of the simulated seasonal changes on the statics solutions derived and applied using autostatics. In Figure 5, as well, we can see the expected reflection amplitude anomaly at about 400ms, but only relatively faint indications of the expected ‘time sag’ anomaly beneath.

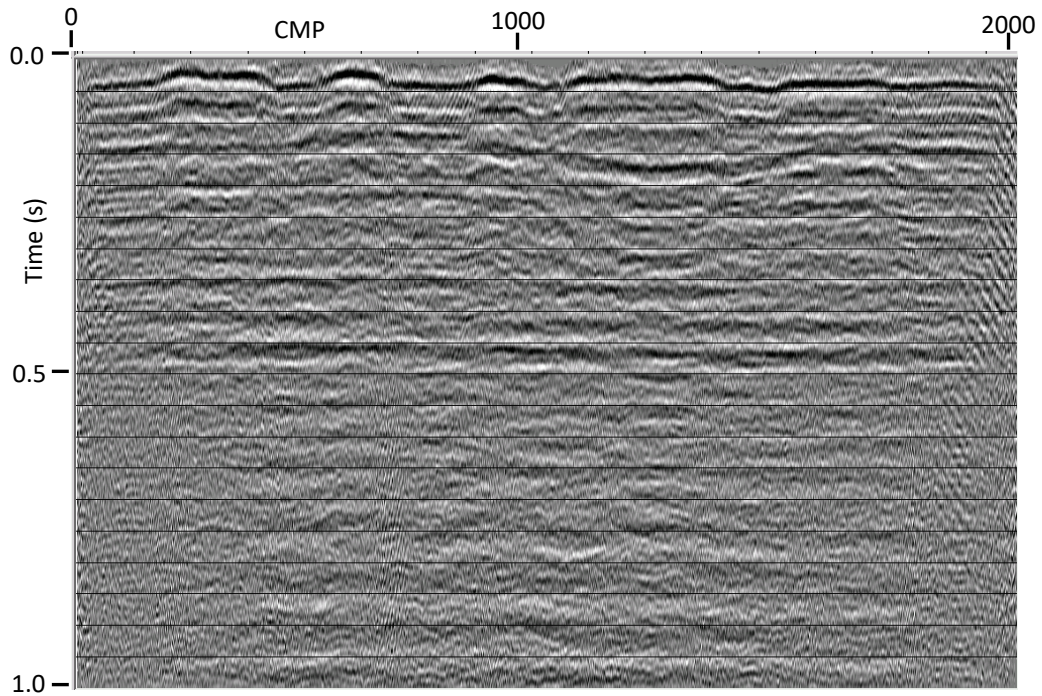


FIG 3. CMP stack of all the processed source gathers for the Baseline model in Figure 1a, after coherent noise attenuation, Gabor deconvolution, NMO correction, and three passes of max-stack-power autostatics.

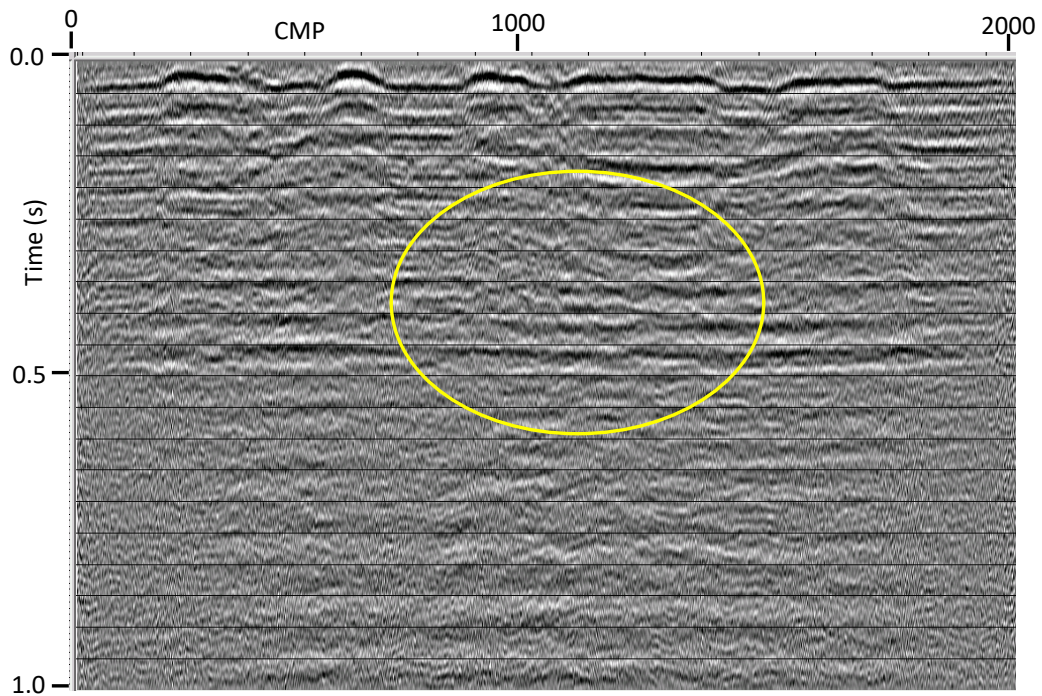


FIG. 4. CMP stack of all the processed source gathers for the Monitor model in Figure 1b, after coherent noise attenuation, Gabor deconvolution, NMO correction, and three passes of max-stack-power autostatics. Yellow ellipse outlines the general area of the expected differences between this image and that in Figure 3.

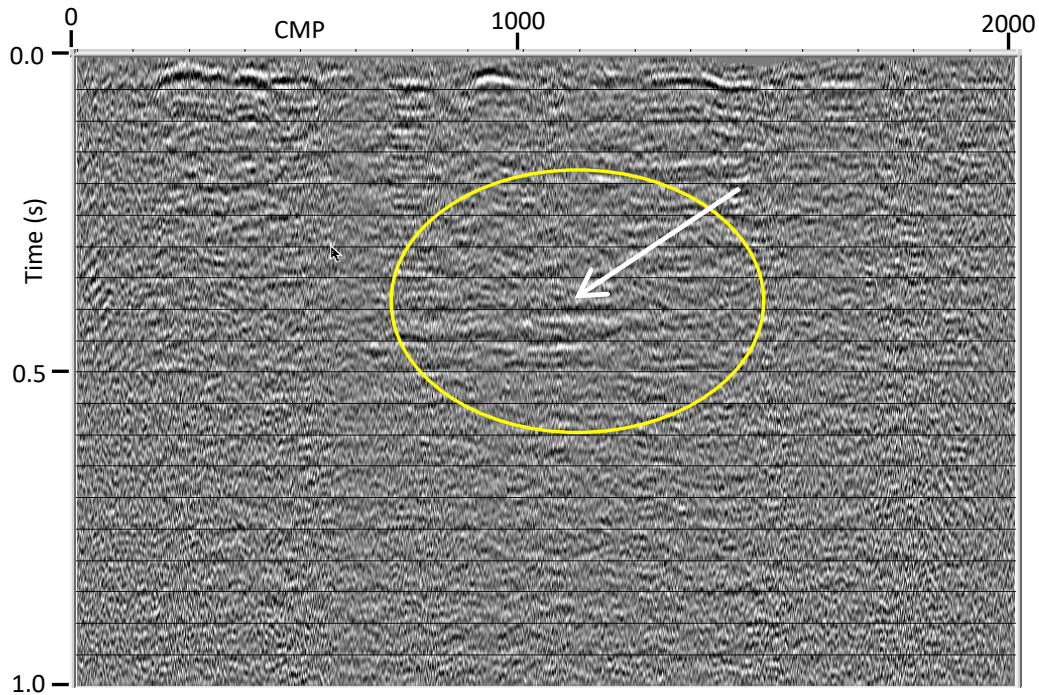


FIG. 5. Subtractive difference between images in Figures 3 and 4. An amplitude anomaly at the position of the simulated fluid injection is clearly visible (arrow), as is a 'time sag' anomaly for the event immediately beneath. Large amplitude, discontinuous events at the surface show the statics differences between the two models, caused by the simulation of seasonal differences. The images in Figures 3 and 4 needed to be shifted by 6ms relative to each other to properly register them before subtraction. This is due to the need to use independent statics solutions for each model (to accommodate the simulated seasonal variations)

To compare autostatics-corrected results with those from raypath interferometry, we used the same radial-trace filtering sequence on the raw source gathers as previously, applied Gabor deconvolution, then applied a single pass of raypath interferometry to each data set, but using the *single* 'reference wavefield' created for the baseline survey to derive and apply the raypath-domain corrections for *both* baseline and time-lapse surveys. After removing the NMO the resulting CMP stack images are shown in Figures 6 and 7, and the difference image in Figure 8. In this case, since the same reference wavefield was used for both data sets, there was no need to shift one image with respect to the other to achieve proper alignment. Interestingly, while we can again see the amplitude anomaly on the difference image, it is the time lag anomaly beneath, that stands out visually, not only immediately beneath the amplitude anomaly, but lateral to the anomaly, and extending to deeper reflections as well. It was this specific result from our numerical modeling experiment that prompted us to try raypath interferometry on field data, to see whether the effect is observable in a field setting.

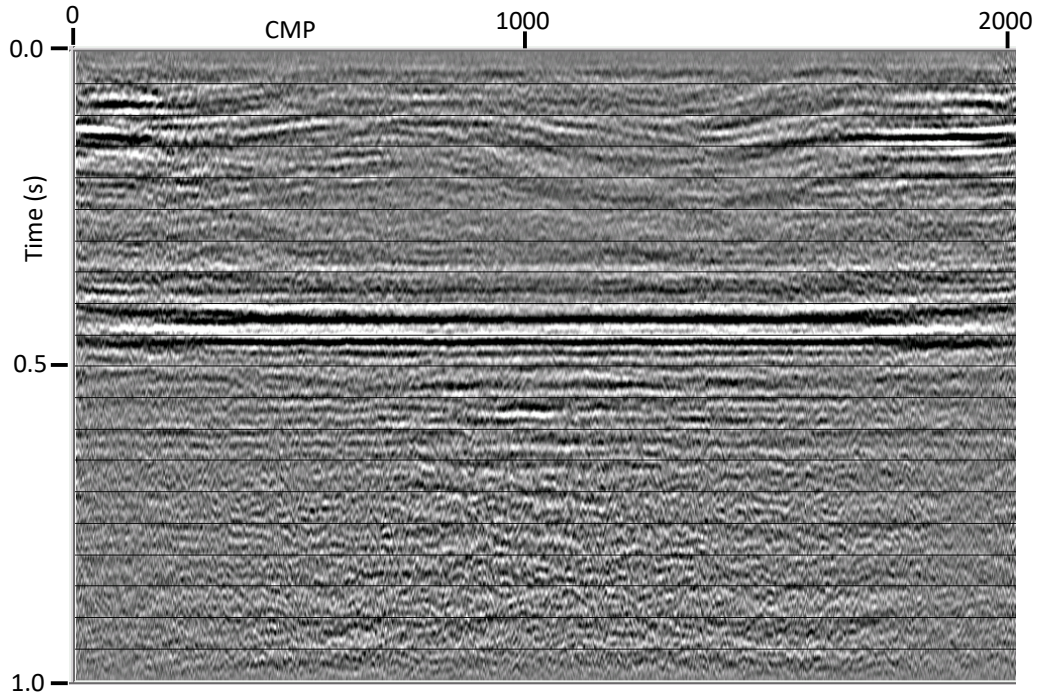


FIG. 6. CMP stack of all source gathers for the Baseline model after coherent noise attenuation, Gabor deconvolution, NMO correction, and raypath interferometry for near-surface corrections.

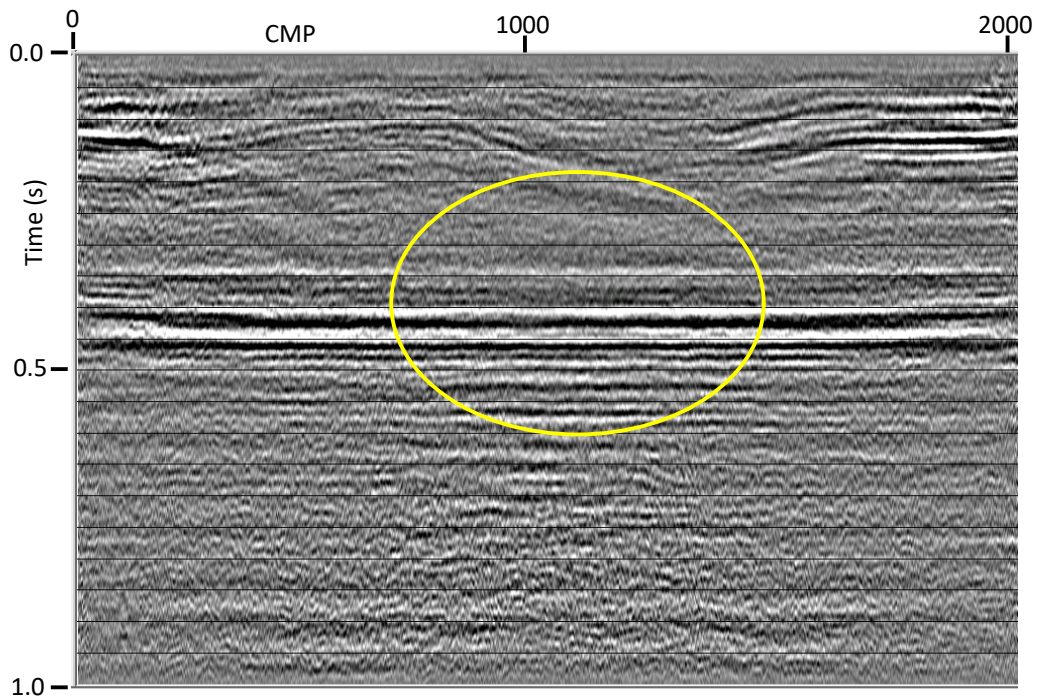


FIG. 7. CMP stack of all source gathers for the Monitor model after coherent noise attenuation, Gabor deconvolution, NMO correction, and raypath interferometry for near-surface correction. Ellipse shows the zone in which we expect to observe differences due to simulated fluid injection.

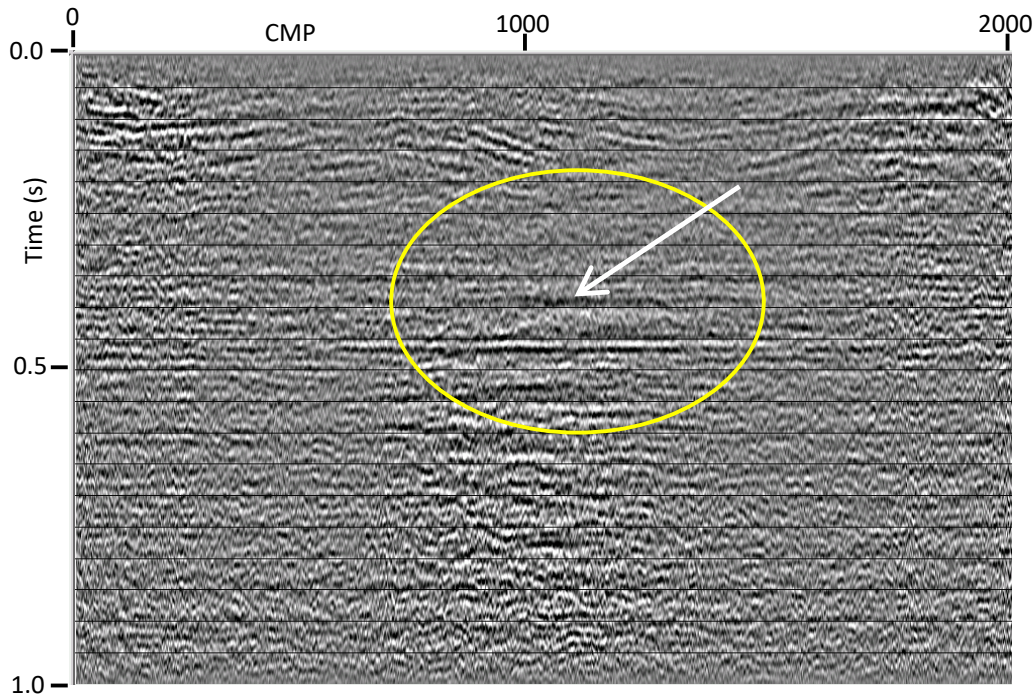


FIG. 8. Subtractive difference between images in Figures 6 and 7. Amplitude anomaly at the level of the simulated fluid injection is visible (arrow), but the time sag anomalies in events beneath the amplitude anomaly are much more prominent. Because raypath interferometry used the same reference wavefield for both Baseline and Monitor models, there is no time shift required to register the images in Figures 6 and 7 before subtraction.

DETECTING THE TIME ANOMALY AT VIOLET GROVE

Several years ago, CREWES was involved in a field test of the time-lapse concept at a producing oilfield in Northern Alberta (Lawton et al 2005, Liu et al 2005, Liu and Lawton 2006, Chen and Lawton 2005, Lu et al 2005, 2006, Alshuhail et al 2007, 2008). Specifically, the field project was intended to test whether seismic techniques could detect a plume of CO₂ injected into a porous formation. A baseline 2D seismic survey was conducted over the field site, centred on the injection well in 2005; then CO₂ injection commenced, and the site was surveyed again in 2007, taking great care to use the exact same surface locations for sources and receivers as in 2005. With both data sets in hand, care was taken to make them as similar as possible by using traces only from source and receiver positions occupied for both surveys, and by processing them as similarly as possible. Various efforts to detect the expected time-lapse amplitude anomaly were made (Alshuhail et al 2007, 2008, Almutlaq and Margrave 2010, 2011, 2012a, 2012b, 2013) through careful processing and creation of difference images. For all these efforts, an amplitude anomaly appeared to be, frustratingly, just at the threshold of definite detection; other features in a difference image were often of similar amplitude to the purported anomaly. Model studies done before the actual survey (Zhang et al 2005, Liu and Lawton 2006) predicted that the reflection amplitude anomaly would be challengingly hard to detect, but also that any time sag caused by velocity changes in the injection zone would be vanishingly small; on the order of fractions of a sample interval. For this reason, a time anomaly was only a secondary objective for the earlier

investigators. After the interesting results we observed above for our numerical modeling results, however, we decided to look for the time sag anomaly on the existing Violet Grove time lapse surveys using interferometry.

The Violet Grove experiment

Violet Grove was the site of a CO₂ sequestration test carried out by Penn West in the 2005-2007 time period in central Alberta (Lawton et al 2005, Liu et al 2005, Liu and Lawton 2006, Chen and Lawton 2005, Lu et al 2005, 2006, Alshuhail et al 2007, 2008), in which CREWES was a participant. Several 2D seismic lines were recorded, in addition to a 2D 3C line and a VSP survey, in 2005, prior to the start of CO₂ injection. These surveys were partially repeated in 2007 after significant injection of CO₂ into the previously depleted Cardium formation. In performing these surveys, care was taken to use the same exact receiver stations in 2007 as in 2005; and the dynamite sources were placed in the same locations, as well, insofar as possible, in order to keep the survey geometry as similar as possible. The objective of CREWES researchers was to detect rock property changes induced by the CO₂ injection by detecting and highlighting differences in the images obtained from the seismic data. Early efforts were focused on Line 1, which straddled the injection well symmetrically. The results of the first analysis were disappointing in that the expected amplitude anomaly at the Cardium level was ambiguous. A later, more sophisticated attempt to highlight survey differences using a matched filter approach (Almutlaq and Margrave 2010, 2011, 2012a, 2012b, 2013) seemed more promising, but results were still not totally convincing.

We use the same Line 1 data sets analyzed by Almutlaq and Margrave; the two vintages of data (2005 and 2007) were reconciled and prepared for comparison as follows:

- Traces from common source points were retained for both the 2005 and 2007 surveys; traces for any source points missing from the 2005 survey were removed from the 2007 survey, and vice versa.
- Similarly, traces corresponding to any dead receivers from the 2005 survey were removed from the 2007 survey and vice versa.
- Source-generated coherent noise was removed from both data sets using the same set of radial trace filters.
- Minimum-phase Gabor Deconvolution was applied to the source gathers of both data sets in single-trace mode, using common parameters.
- The deconvolved traces of both data sets were zero-phase bandlimited to a common band.
- A single NMO velocity function was determined by visual moveout analysis of the 2005 source gathers, for later use on both data sets.

These steps were intended to ensure that the two data sets were as identical as possible, with the exception of weathering effects (expected to vary with the acquisition date) and effects due to the injection-induced anomaly itself. Although the sources for both surveys were dynamite charges of the same size and depth, some variability of source spectrum was expected; but it was also expected that this variability would be relatively random across both surveys, with no systematic variation between the two vintages of survey. The application of Gabor Deconvolution coupled with zero-phase bandlimiting was expected to make the source spectra more uniform across the two data sets. Besides using identical parameters for deconvolution and bandlimiting, no attempt was made to preserve true reflection amplitudes, since the objective of our research was to investigate event transit time differences rather than amplitude differences, as in previous studies (Alshuhail and Lawton 2007, Alshuhail et al 2008).

A detectability experiment

Since it was an interferometry experiment on synthetic data that attracted our attention to the possibility of detecting subtle time lags between events on time-lapse surveys (Figure 8), we constructed a simulation based on the 2005 Violet Grove survey to investigate the detectability of very small time shifts between events on actual field data. The test was conducted as follows:

- Raypath interferometry was applied to all the source gathers of the 2005 survey, using smoothed gathers from the 2005 survey as a reference wavefield and using the Tau-P transform to move to/from the ray-parameter domain (Cova et al 2015).
- A relatively high level of bandlimited Gaussian noise was added to all the traces in each source gather.
- The pre-determined NMO velocity function was used to remove NMO from all the source gathers.
- The CMP stack image of all the gathers was formed.
- Small time shifts (0.5ms) were applied to all stack traces with CMP between 325 and 375, to simulate a ‘vertical incidence’ time-lapse survey.
- The original CMP stack was subtracted from the ‘time-lapse’ CMP stack.
- As a check, the original CMP stack was time-shifted by 0.5ms and subtracted from the ‘time-lapse’ CMP stack.
- The test was performed for two different levels of additive noise

Figure 9 shows one of the source gathers from the 2005 survey after raypath interferometry, with RMS S/N = 0.2. Figure 10 is the CMP stack image of the complete 2005 survey, while Figure 11 is the image of the survey with 0.5ms time shifts applied to all traces between CMPs 325 and 375. As we would expect, we can see no real visible

difference between these images. The difference image in Figure 12, however, shows that this small time shift is readily detectable. Confirmation is supplied by Figure 13, which shows the time-lagged ‘baseline’ survey subtracted from the ‘time-lapse’ survey; here, the time differences show up everywhere *except* in the anomalous zone. When we repeat this experiment for a higher noise level (RMS S/N = 0.1), with the source gather shown in Figure 14, the CMP stack images (Figures 15 and 16) are truly indistinguishable visually; but the difference images (Figures 17 and 18) still highlight the ‘anomalous’ zone.

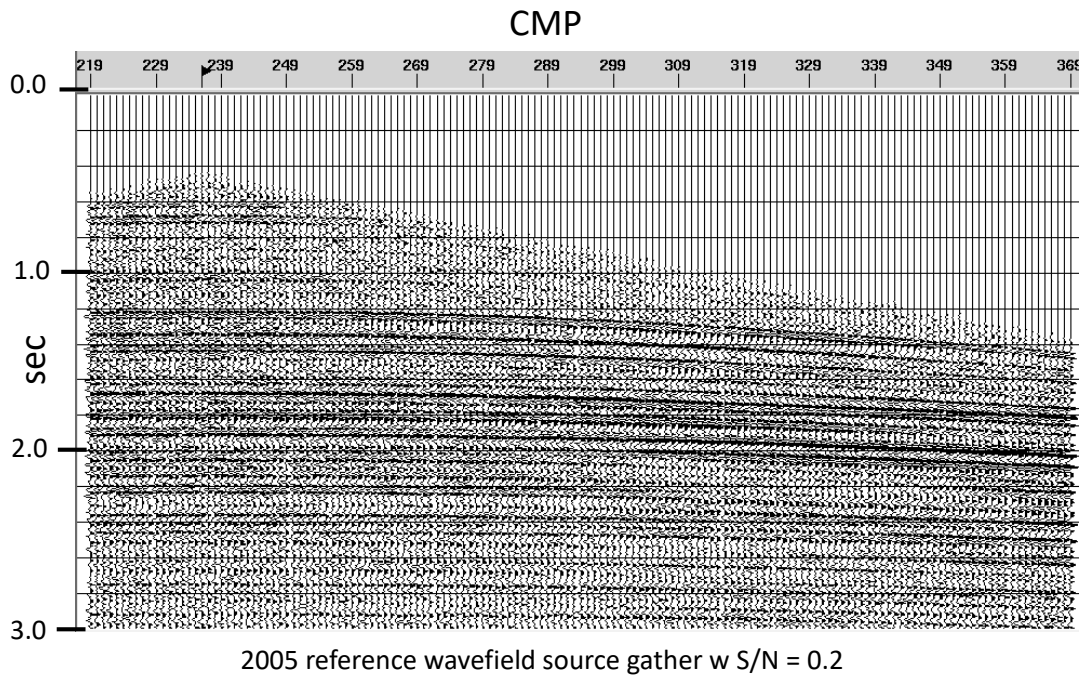


FIG. 9. Source gather from the 2005 Violet Grove survey reference wavefield, with added bandlimited random noise of RMS S/N = 0.2. All such 2005 gathers were used as a model to test for detectability of small time shifts.

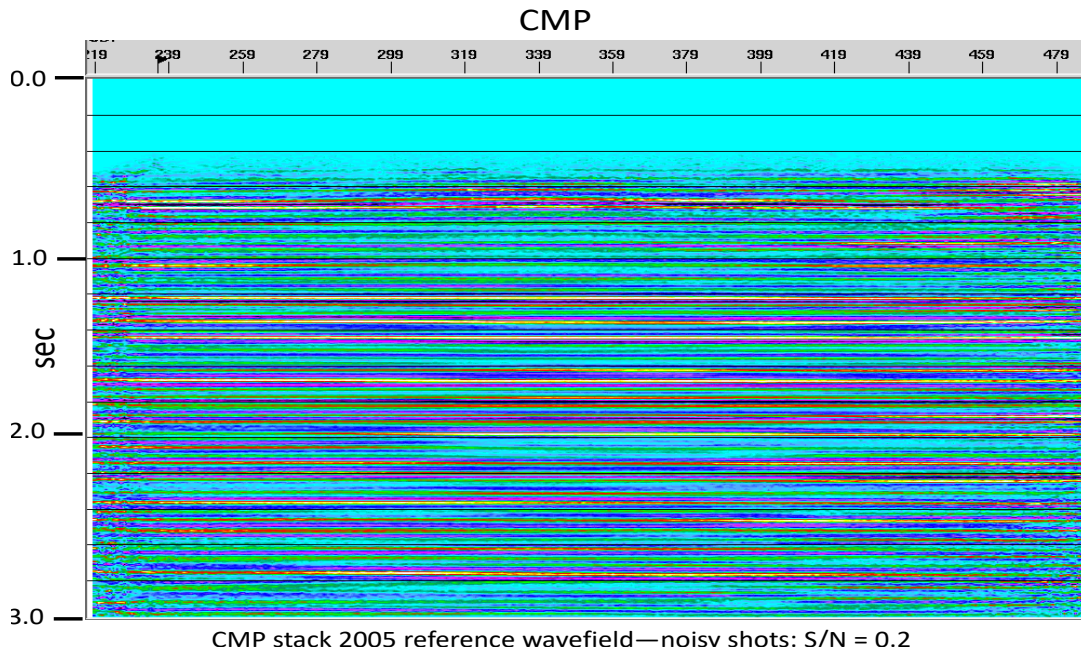


FIG 10. CMP stack of all noisy 2005 source gathers for the Violet Grove time shift detection simulation.

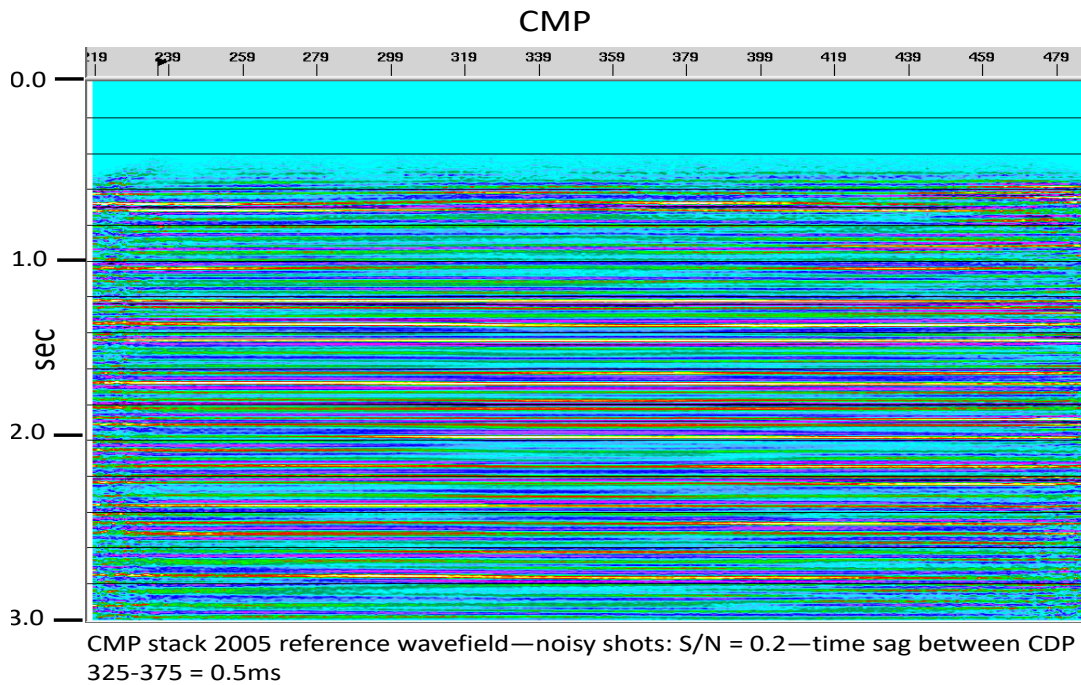


FIG 11. CMP stack of all noisy 2005 source gathers for the Violet Grove time shift detection simulation, with 0.5ms shift applied to all traces between CMPs 325 and 375. Visual comparison with Figure 10 shows no discernible difference.

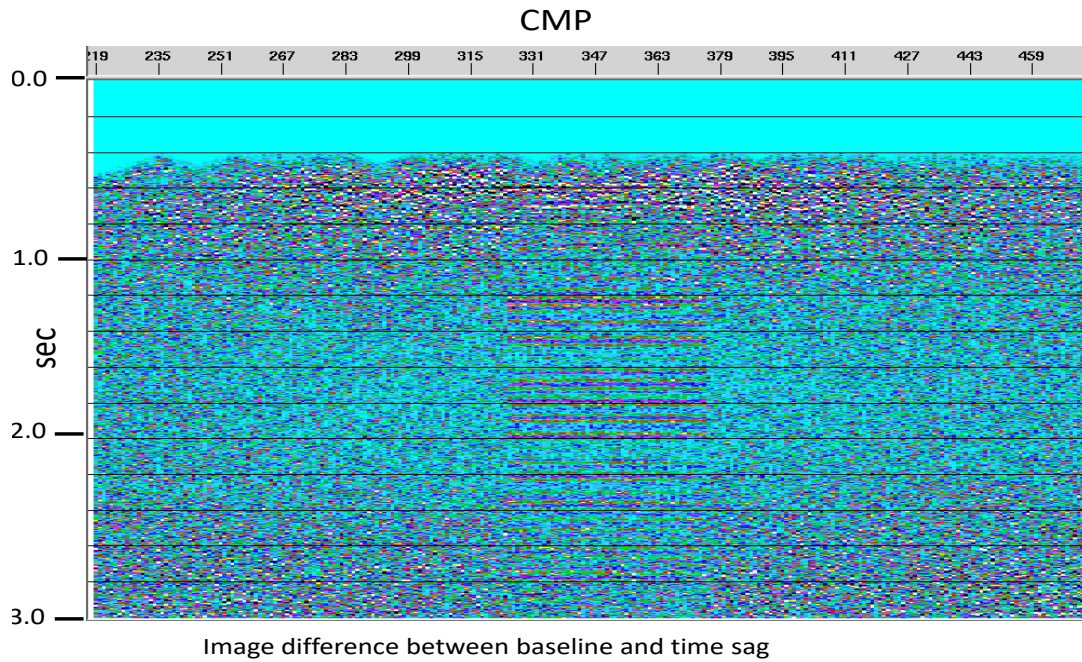


FIG. 12. Subtractive difference between images in Figures 10 and 11. The 0.5ms time shift is easily visible.

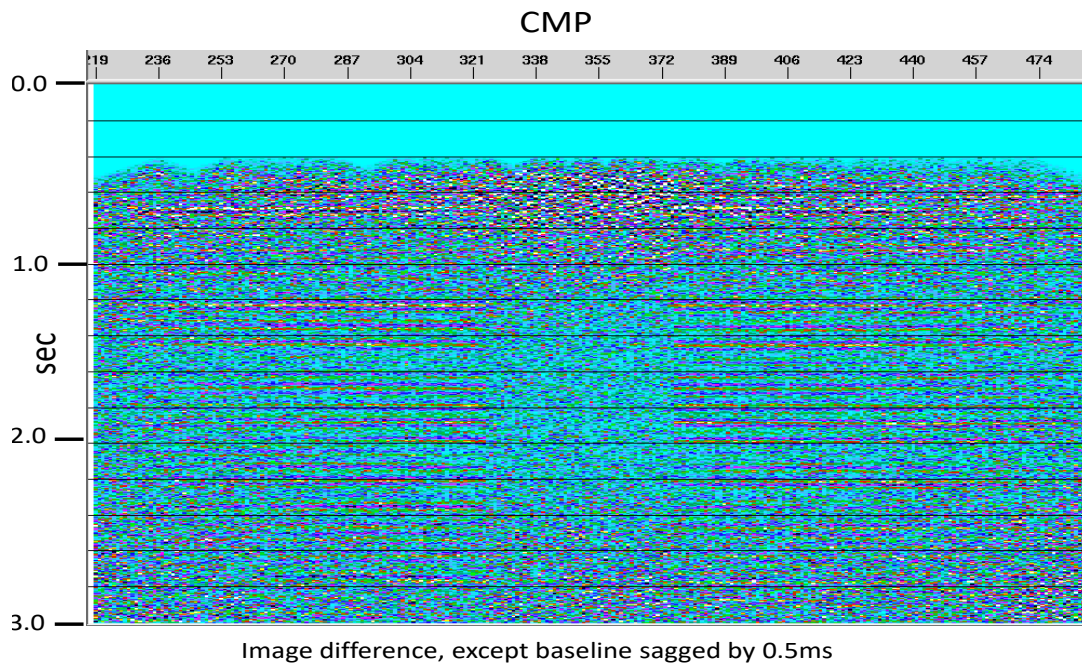
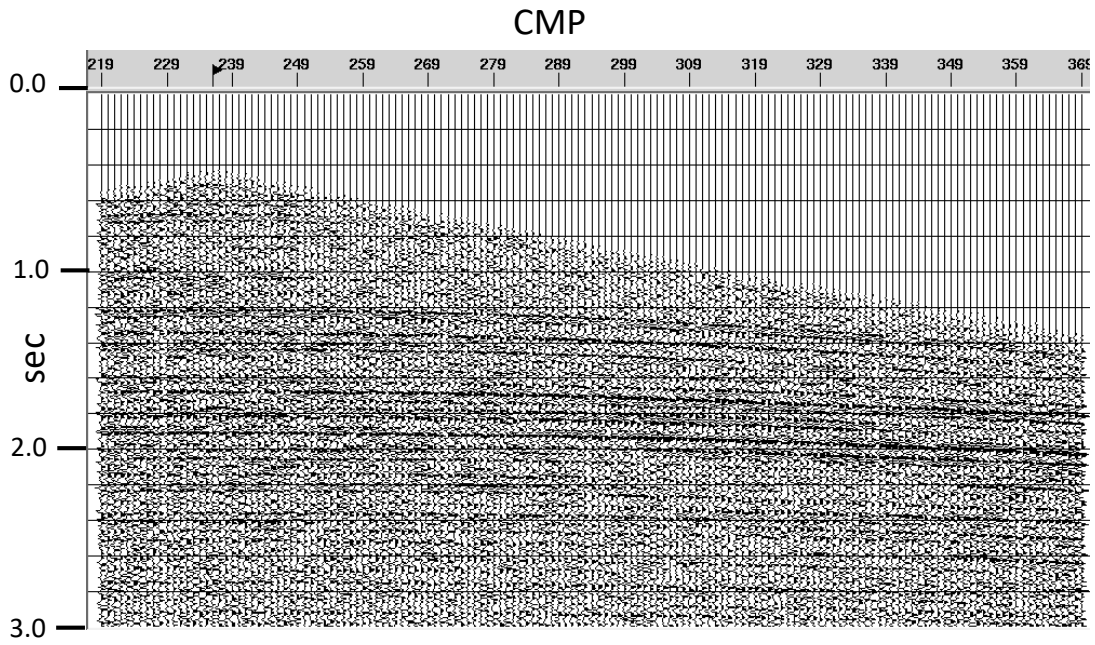
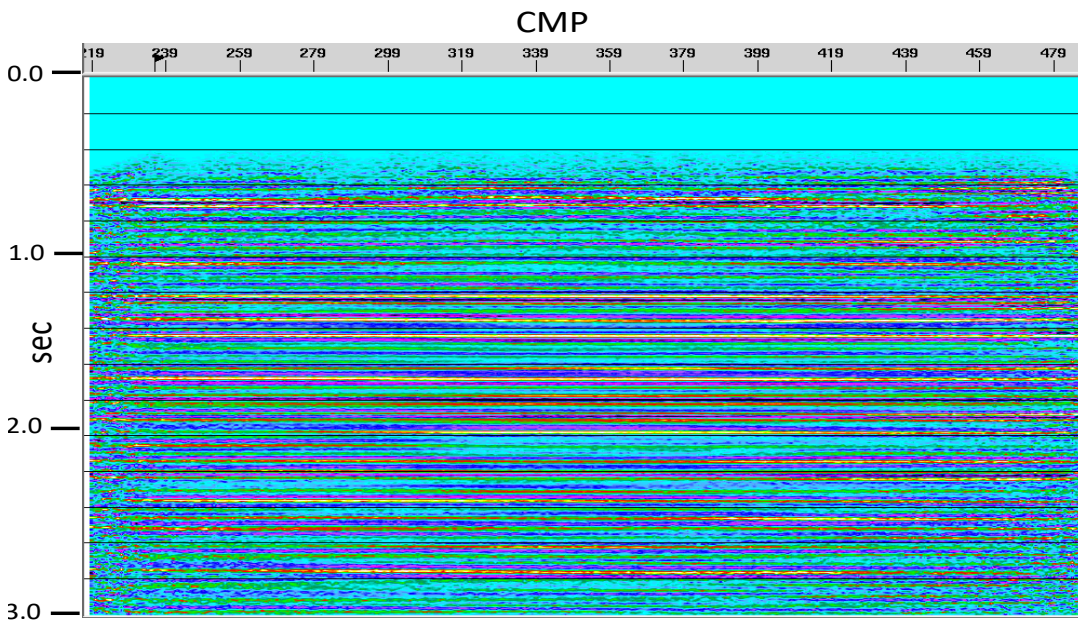


FIG. 13. Subtractive difference between Figures 10 and 11, but with 0.5ms shift applied to all traces in Figure 10. The time-shifted zone now appears as a null zone.



2005 reference wavefield source gather w $S/N = 0.1$

FIG. 14. 2005 source gather for the time difference detectability experiment with additive bandlimited noise level of RMS $S/N = 0.1$. Some events are difficult to see at this noise level.



CMP stack 2005 reference wavefield—noisy shots: $S/N = 0.1$

FIG. 15. CMP stack image of all 2005 source gathers with $SN = 0.1$ for time shift detectability experiment.

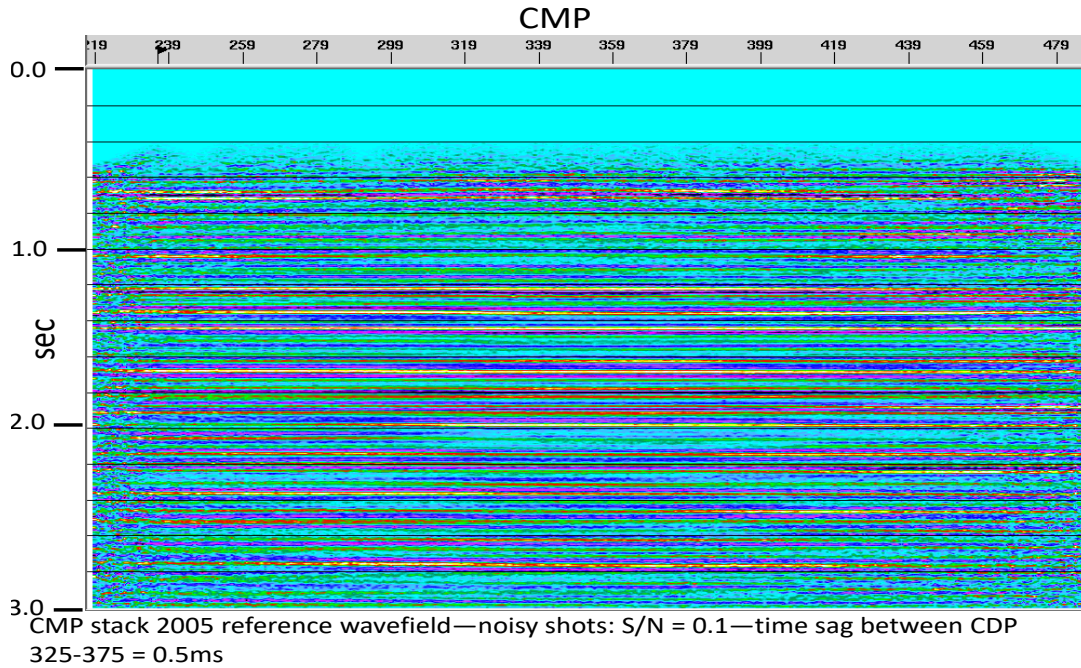


FIG. 16. Same as Figure 15, but with all traces for CMPs 325 – 375 shifted by 0.5ms. No visible differences between this figure and Figure 15.

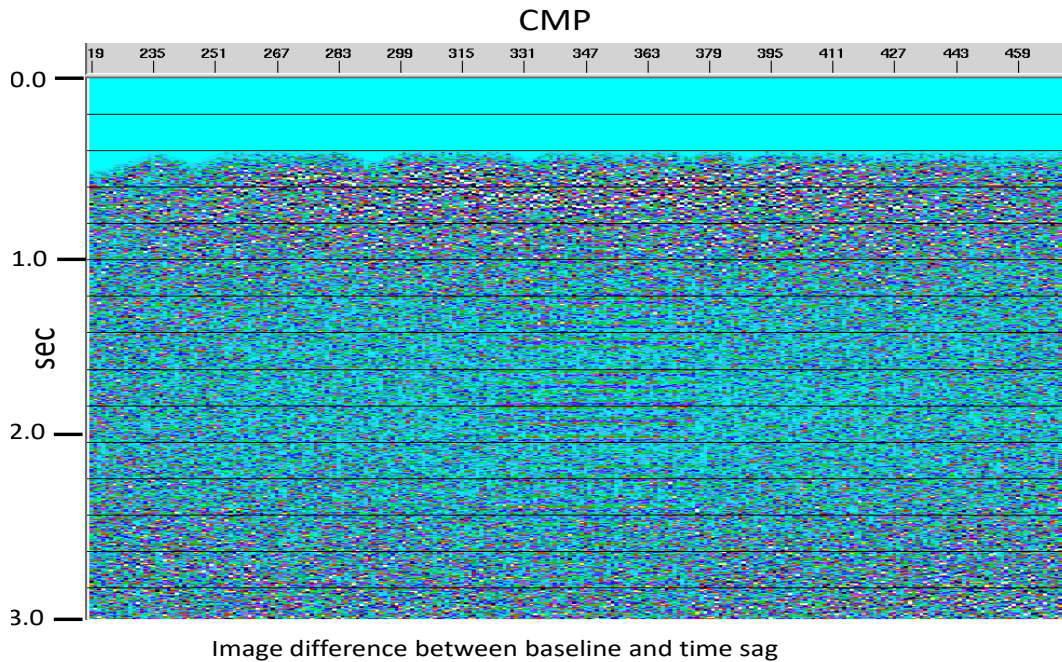


FIG. 17. Subtractive difference between the images in Figures 15 and 16. Time shifts on events between CMPs 325 and 375 still visible, even at this higher noise level.

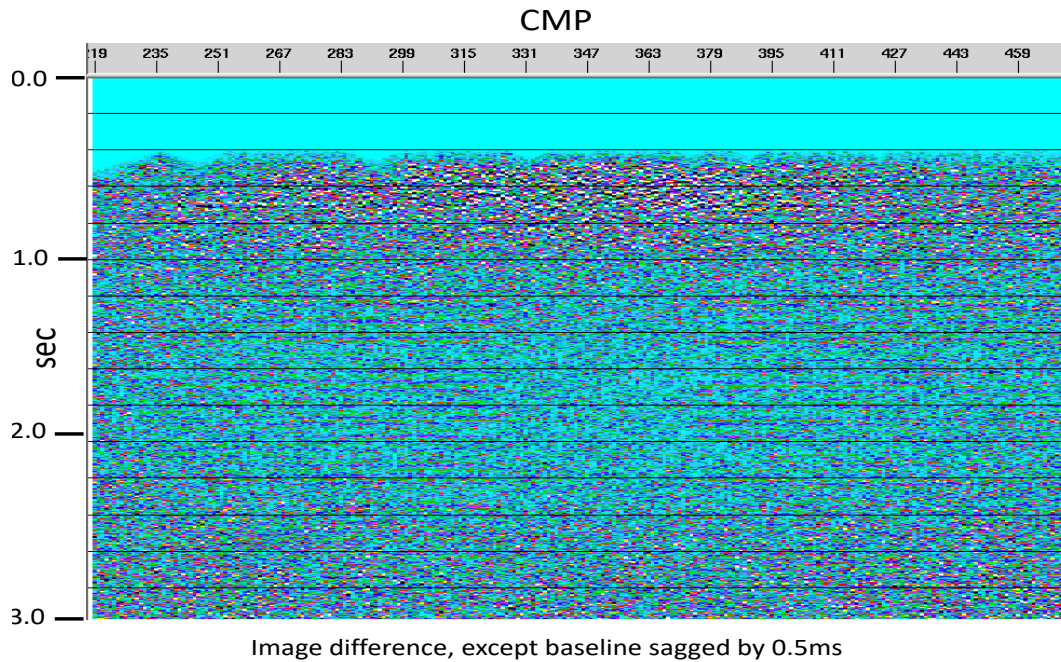


FIG. 18. Same as Figure 17, except all traces in the image in Figure 15 shifted by 0.5ms before subtraction. The null zone for CMPs between 325 and 375 once again confirm that this small time shift is detectable even in the presence of significant random noise on the input source gathers.

This experiment convinced us that we should be able to detect systematic time lags, whose magnitude is much less than a sample interval, between portions of two nearly identical images. One difference we expect to see when actually doing the time-lapse test, however, is that the lateral extent of the anomalous time lag zone should increase with depth. This is just a reflection of the fact that raypaths penetrate the anomalous zone at all angles, rather than just at vertical incidence, and the corresponding traces contribute to CMPs whose locations move away from the edges of the anomaly with increasing depth, unlike the simplistic ‘vertical incidence’ simulation of our test.

Processing details

The preliminary stages of processing for both the 2005 baseline survey from Violet Grove and the 2007 time-lapse survey are described above. These differ significantly from the processing applied by Almutlaq and Margrave (2012b) in their application of matched filtering to delineate time-dependent differences between the two vintages of survey. Specifically:

- We applied radial trace filters to attenuate all linear coherent source-generated noises, not just ground roll.
- We applied severe initial muting to all traces in order to eliminate the relatively variable shallow data, which contains not only a strong reflection (the Ardley Coal), but also residual coherent noise.

- Instead of standard amplitude recovery, surface-consistent amplitude recovery and surface-consistent spiking decon, we applied single-trace minimum-phase Gabor Deconvolution to all traces, followed by zero-phase bandlimiting to attenuate high-frequency noise introduced by the Gabor Deconvolution.
- We did not derive and apply surface-consistent residual statics to either data set, since raypath interferometry replaces this procedure.

With respect to the second bullet point above, we experimented with various amounts of initial muting, including no muting whatever, and we found that the CMP stack difference image tended to exhibit the largest difference amplitudes in the shallow portion of the image. As we increased the muting, we found that these difference amplitudes could be reduced to insignificance with the proper choice of muting applied to both data sets. Figure 19 shows a single source gather from the 2005 baseline survey after coherent noise attenuation, Gabor deconvolution, and zero-phase filtering, with no muting, while Figure 20 shows the corresponding source gather from the 2007 time-lapse survey, with the same processing. It can be seen on these figures that the residual direct arrival and refracted near-surface energy surviving the coherent noise attenuation is still strong in amplitude, although not very coherent. Figure 21 is the difference between the CMP stacks for the two surveys. Note that the portion of the image between 0 and 800ms is dominated by strong amplitudes due to the residual coherent noises that have survived the attenuation process. In the presence of these amplitudes, it is difficult to decide which amplitude differences deeper in the image are legitimate. Figures 22 and 23, on the other hand show the same source gathers as Figures 19 and 20, but with initial muting applied. Figure 24 shows the CMP stack difference for the data sets when muted as shown in Figures 22 and 23, and it is apparent that the most significant amplitude differences in this image now occur in the zone of our interest. Having removed the distraction of the amplitude differences in the shallow portion of the section, we refine the details of the raypath interferometry, whereby we hope to detect reflection transit time differences induced by the injection of CO₂ at this test site.

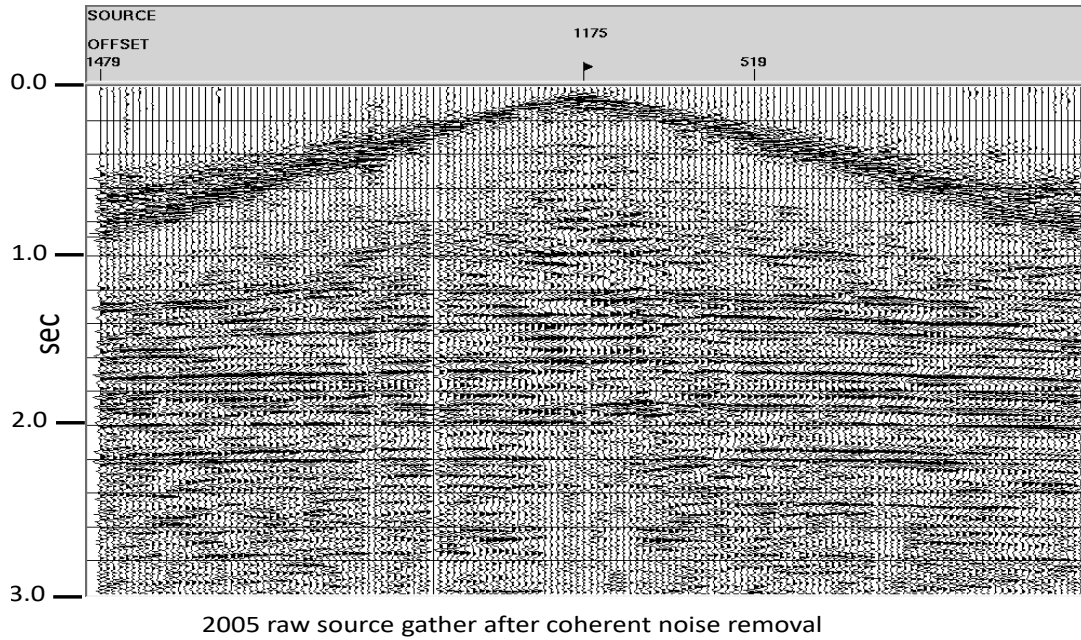


FIG. 19. Source gather from Violet Grove 2005 survey after coherent noise attenuation, Gabor deconvolution, and zero phase bandlimiting.

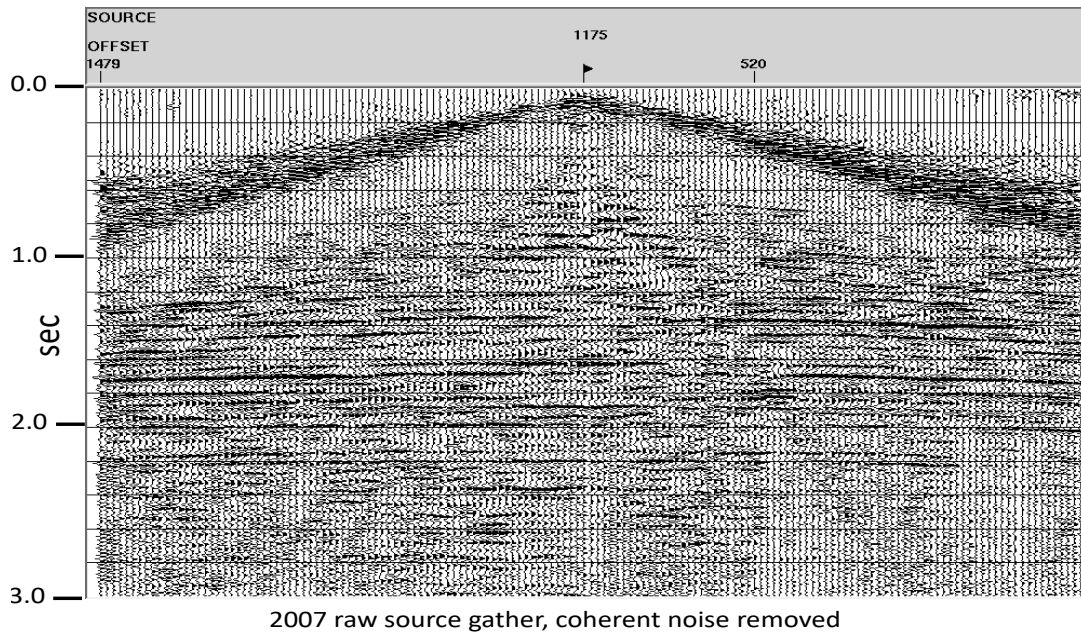


FIG. 20 Comparable source gather from the Violet Grove 2007 survey, same processing.

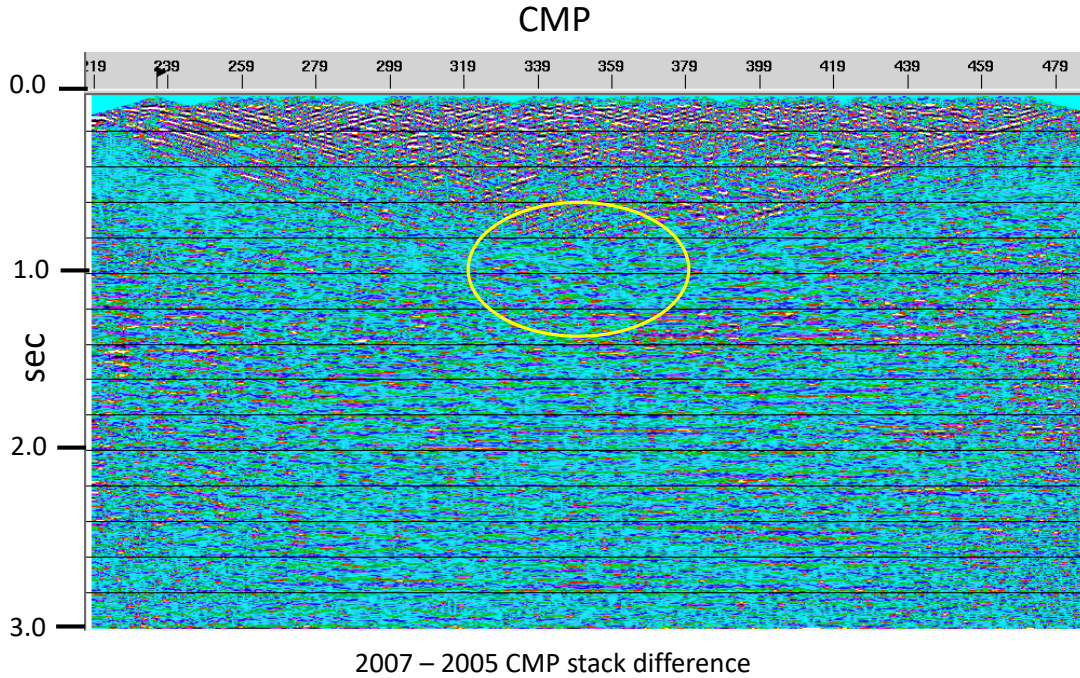


FIG. 21. Subtractive difference between CMP stacks for 2007 and 2005 Violet Grove surveys. Ellipse marks the potential amplitude anomaly zone. Amplitude differences caused by residual coherent noise in shallow section overwhelm any deeper anomalies.

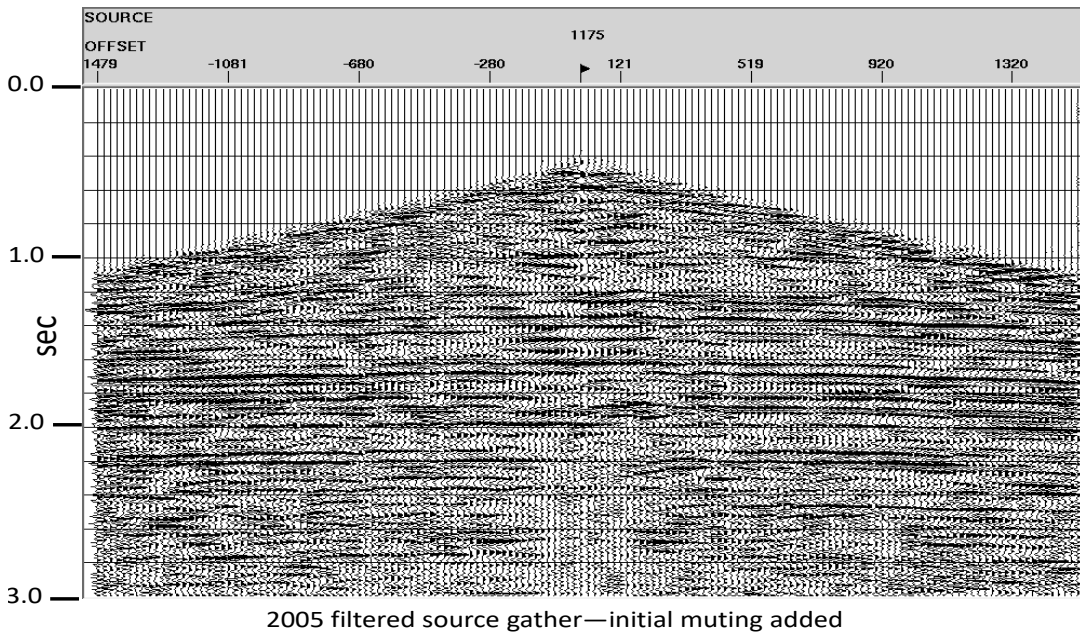


FIG. 22. 2005 source gather from Figure 19, with initial muting applied to eliminate coherent noise residuals.

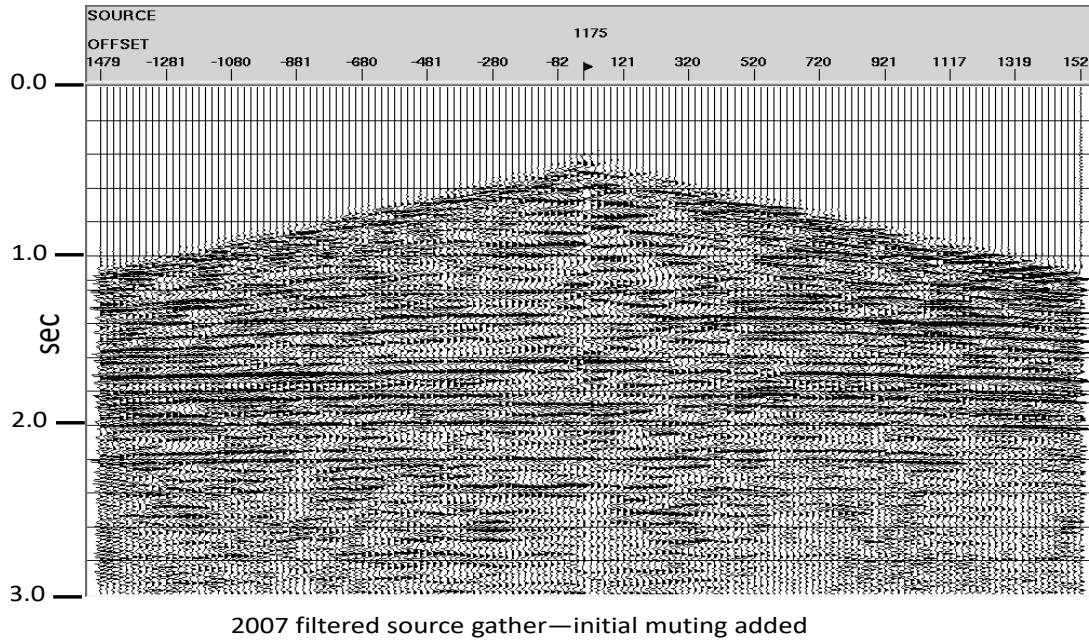


FIG 23. 2007 source gather from Figure 20 with same initial muting as Figure 22, to eliminate coherent noise residuals.

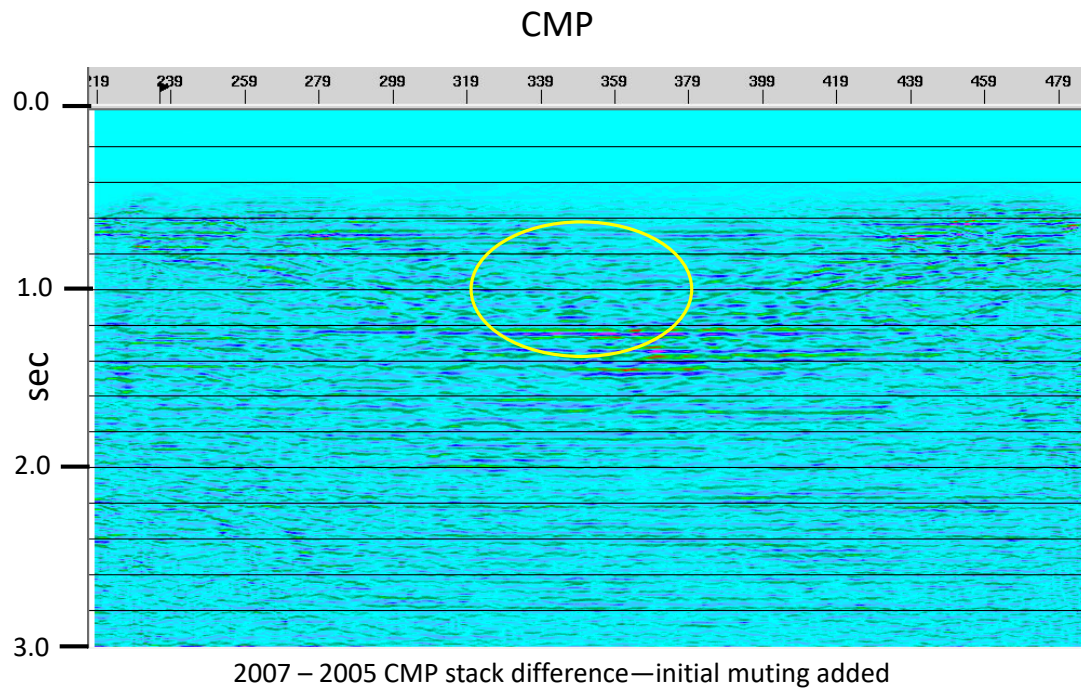


FIG. 24. Subtractive difference between CMP stacks for 2007 and 2005 Violet Grove surveys. Ellipse marks the potential location of amplitude anomaly associated with CO₂ injection at this location. Shallow amplitude differences due to residual coherent noise are not present in this image, since initial muting of all source gathers has removed this distraction. Even in this preliminary image, we see intriguing hints of a possible time-sag anomaly.

Raypath interferometry details

The basics of raypath interferometry were introduced by Henley (2012a, 2012b) and improved by Cova et al (2015). Based on Cova's experience with the Tau-P transform, we decided to use it instead of the Radial Trace Transform for moving to and from the ray-parameter domain in this study.

The idea behind the use of raypath interferometry in the time-lapse setting is that we can use a common wavefield estimate (pilot traces) to derive and apply surface functions to both data sets. In the raypath interferometry technique, data are transformed to the raypath domain and organized into raypath/surface-location order. This means that the trace-to-trace cross-correlations computed against the wavefield estimate traces (also organized into raypath/surface-location order) apply corrections pertinent only to raypath and surface location, rather than CMP location. If the same estimated wavefield is used for applying raypath interferometry to each survey, all reflections on both surveys are independently corrected in a non-stationary way. Hence any actual reflection time differences between corresponding events on the two surveys is properly preserved. Using a common estimated wavefield (we use the estimate from the baseline survey) has the additional advantage of forcing the two data sets to be exactly registered in transit time for comparison by subtraction, unlike independently applied autostatics solutions, which can leave the survey CMP images misaligned in transit time due to differences in the statics solutions caused by seasonal and acquisition differences.

The processing steps involved in preparing the CMP stack sections for time-lapse/baseline comparison are as follows—all program parameters are the same for both data sets:

- NMO was removed from all the source gathers of the 2005 baseline survey.
- Trace mixing and eigenvector filtering were applied to all source gathers of the 2005 baseline survey to form the estimated wavefield.
- NMO was reapplied to the 2005 baseline source gathers, as well as the estimated wavefield source gathers.
- The Tau-P transform was applied to each of the 2005 baseline source gathers, using parameters designed to maximize lateral resolution.
- The Tau-P traces of the estimated wavefield were sorted into ray-parameter/surface-location order, as common-ray-parameter gathers.
- The Tau-P traces of the raw 2005 baseline survey were also sorted into ray-parameter/surface-location order, as common-ray-parameter gathers.
- Common-ray-parameter gathers of the estimated wavefield were matched with common-ray-parameter gathers of the 2005 baseline survey with the same ray-parameter.

- Corresponding traces of each pair of common-ray-parameter gathers were cross-correlated, the correlations whitened and windowed (Henley, 2012a).
- The ‘conditioned’ correlation functions were used to derive inverse filters, each of which was convolved with its corresponding common-ray-parameter trace from the 2005 baseline survey to apply the near-surface correction.
- The Tau-P traces of the 2005 baseline survey were re-sorted back into surface-location/ray-parameter order and transformed back to ‘corrected’ 2005 source gathers.
- NMO was removed from the ‘corrected’ 2005 baseline source gathers, and the traces were stacked by CMP.
- Using the same parameters as for the 2005 baseline survey, the Tau-P transform was applied to each of the source gathers in the 2007 time-lapse survey, and the resulting traces sorted by ray-parameter/surface-location.
- As with the 2005 baseline survey, all common-ray-parameter gathers from the 2007 time-lapse survey were matched by ray-parameter with their corresponding common-ray-parameter gathers in the ‘estimated wavefield’ computed previously for the 2005 baseline survey.
- Corresponding traces of each pair of common-ray-parameter gathers were cross-correlated, the correlations whitened and windowed.
- The ‘conditioned’ correlations were used to derive inverse filters, which were used to ‘correct’ the common-ray-parameter traces of the 2007 time-lapse survey.
- The Tau-P traces of the 2007 time-lapse survey were re-sorted back to surface-location/ray-parameter order and transformed back to ‘corrected’ 2007 source gathers.
- The same NMO function was removed from the ‘corrected’ 2007 time-lapse gathers, and the traces were stacked by CMP.

The above procedure resulted in two CMP stack sections to be compared for transit time anomalies due to injection operations at the Violet Grove test site. Figure 25 shows one source gather of the estimated wavefield computed from the 2005 baseline survey, while Figure 26 displays its Tau-P transform. Note that the transform requires several times the storage space of the input source gather, necessitated by the lateral resolution requirement. Figure 27 illustrates one common-ray-parameter gather of the estimated wavefield. Figure 28 shows the Tau-P transform of the raw 2005 baseline source gather for the same surface location, while Figure 29 shows the corresponding common-ray-parameter gather for the 2005 baseline survey. Typical correlation functions between a baseline common-ray-parameter gather and its corresponding estimated wavefield common-ray-parameter gather are shown in Figure 30. The common-ray-parameter

gather in Figure 29 is shown again in Figure 31 after application of the inverse filters which correct for the correlations shown in Figure 30. Figure 32 shows the Tau-P transform in Figure 28 after correction, and Figure 33 shows the original 2005 source gather (inverse Tau-P transform) after correction. Figures 34 and 35 show the resulting CMP stacks for the 2005 baseline and 2007 time-lapse surveys, respectively, where the same processing was applied to each data set, the 2005 estimated wavefield being used in both cases.

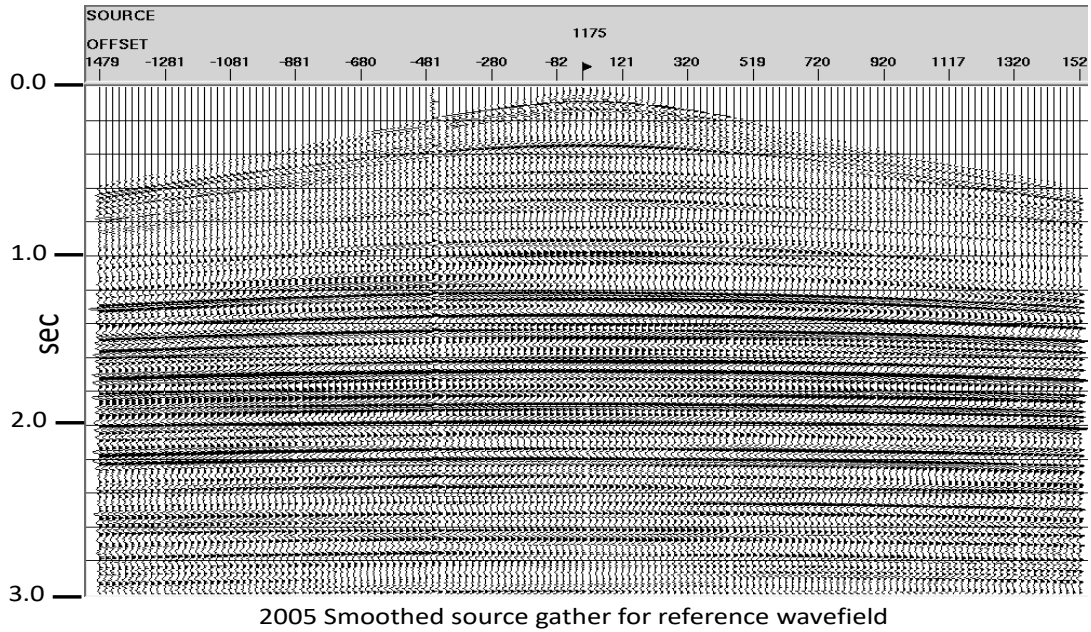


FIG. 25. Example of a 'reference wavefield' source gather created from the 2005 Violet Grove 'Baseline' survey.

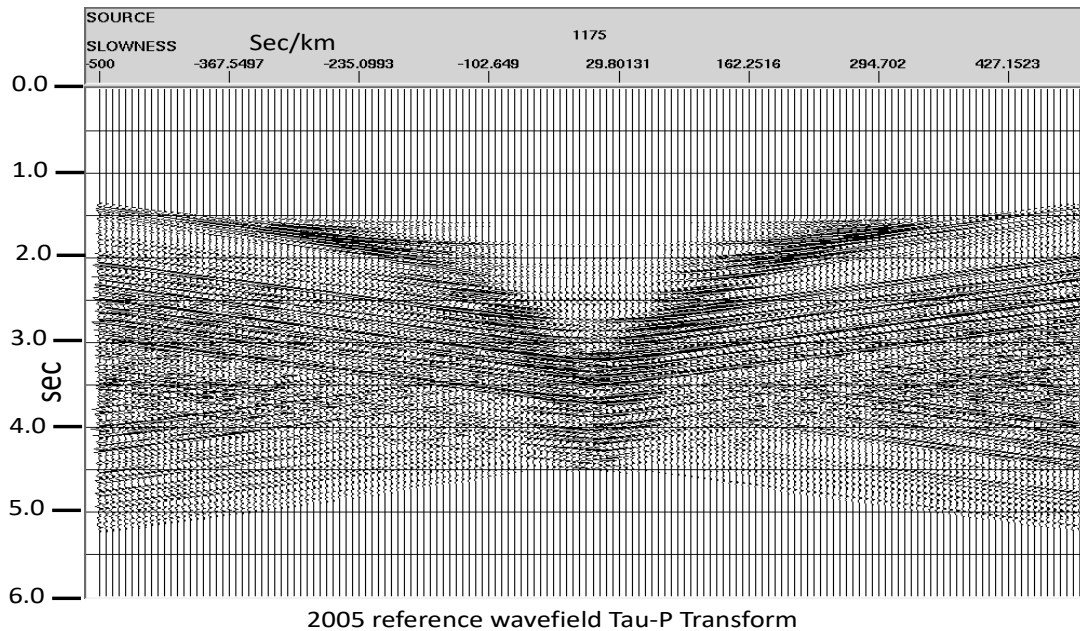


FIG. 26. Tau-P transform of the reference wavefield source gather in Figure 25. The time scale shows that this gather requires several times the storage space of the original X/T gather in Figure 25.

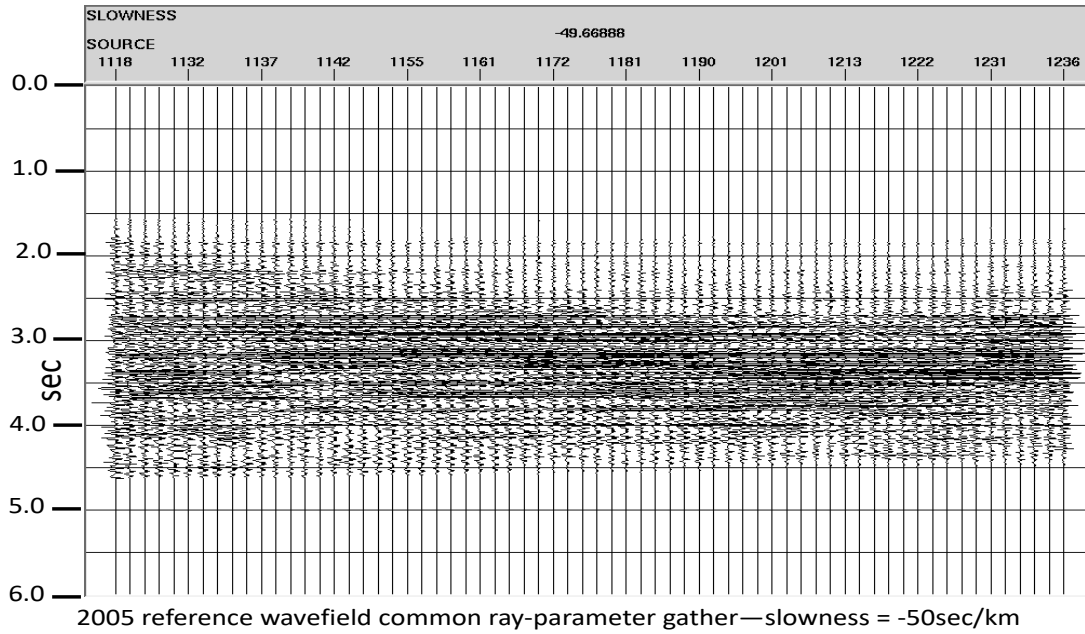


FIG. 27. Example of a common-ray-parameter gather for the 2005 reference wavefield—slowness = -50 sec/km (ray-parameter).

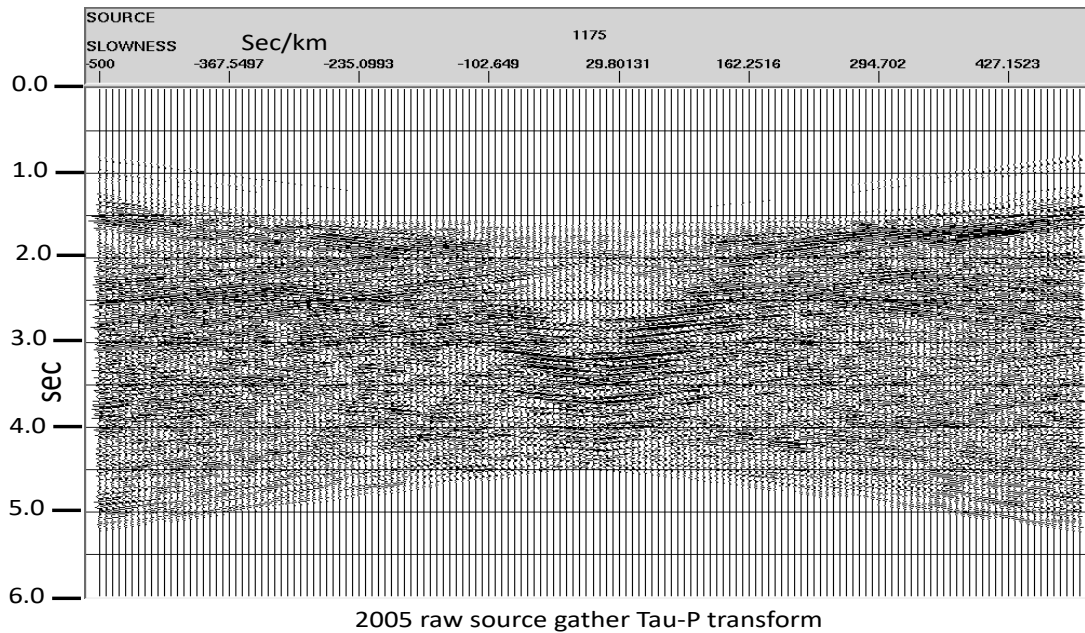


FIG. 28. Tau-P transform of the processed source gather corresponding to the same source point as Figure 26.

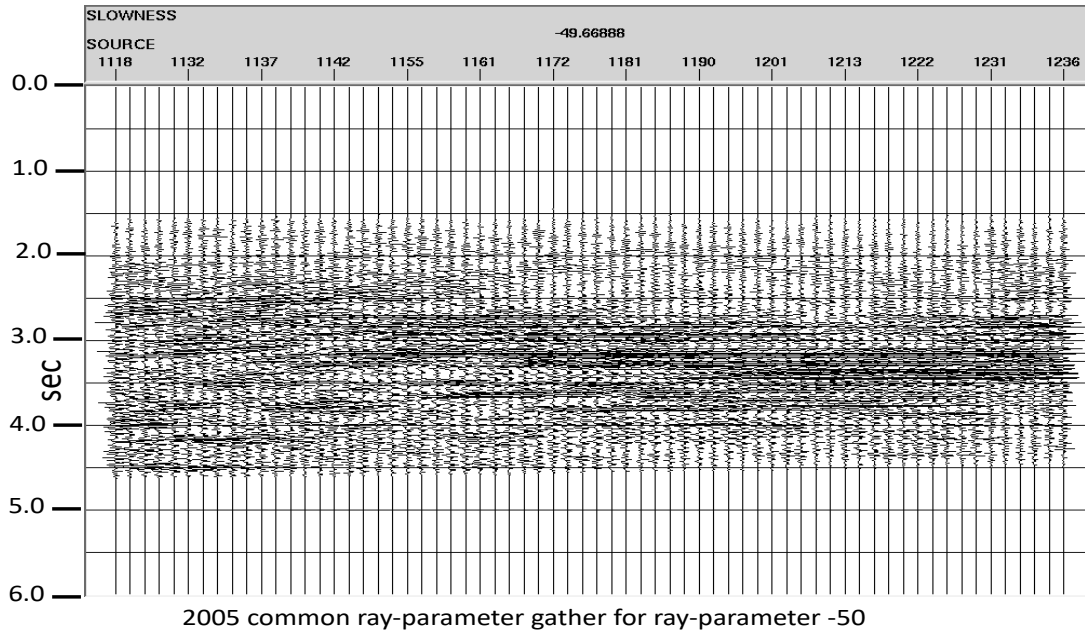


FIG. 29. Common-ray-parameter gather for 2005 Violet Grove survey for slowness = -50sec/km (ray-parameter)..

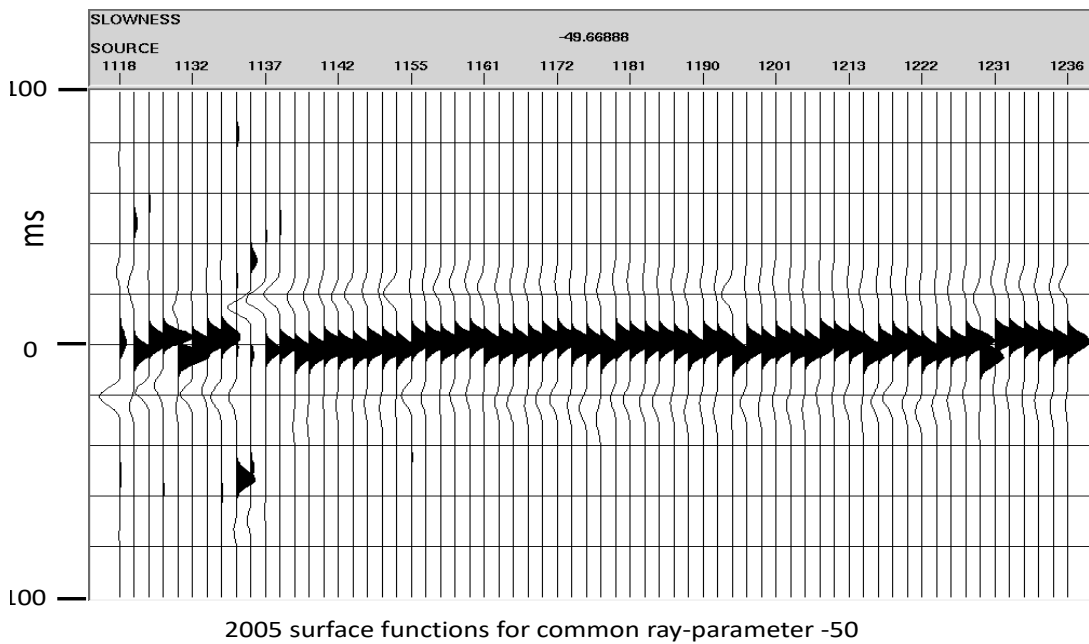


FIG. 30. Surface functions for 2005 Violet Grove survey for slowness = -50sec/km (ray-parameter), generated by cross-correlating the traces in Figures 27 and 29.

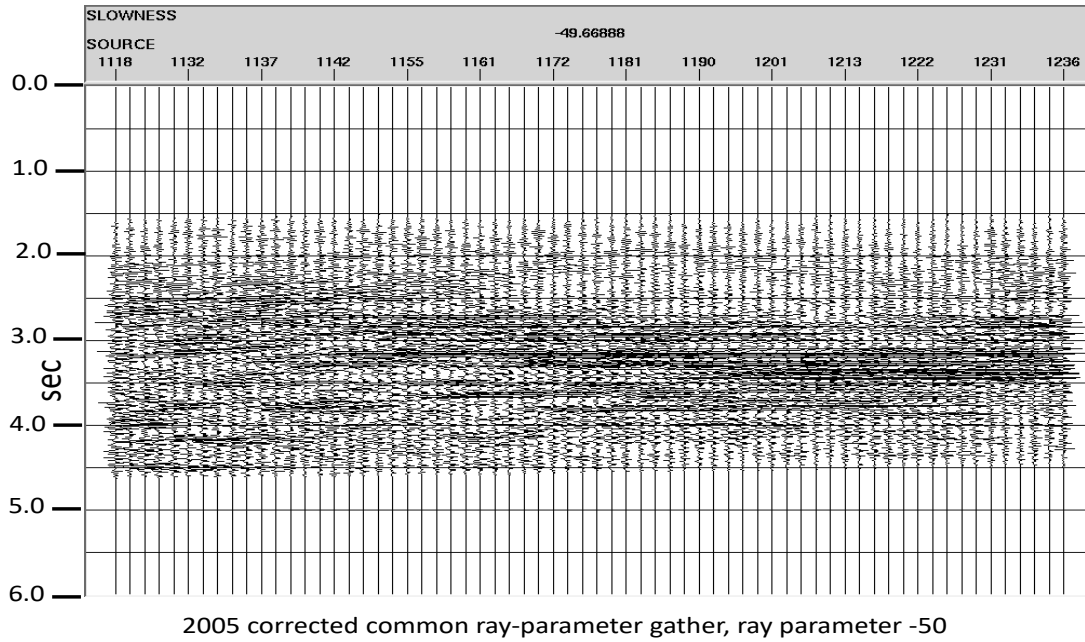


FIG. 31. Common-ray-parameter gather from Figure 29 after application of surface functions in Figure 30.

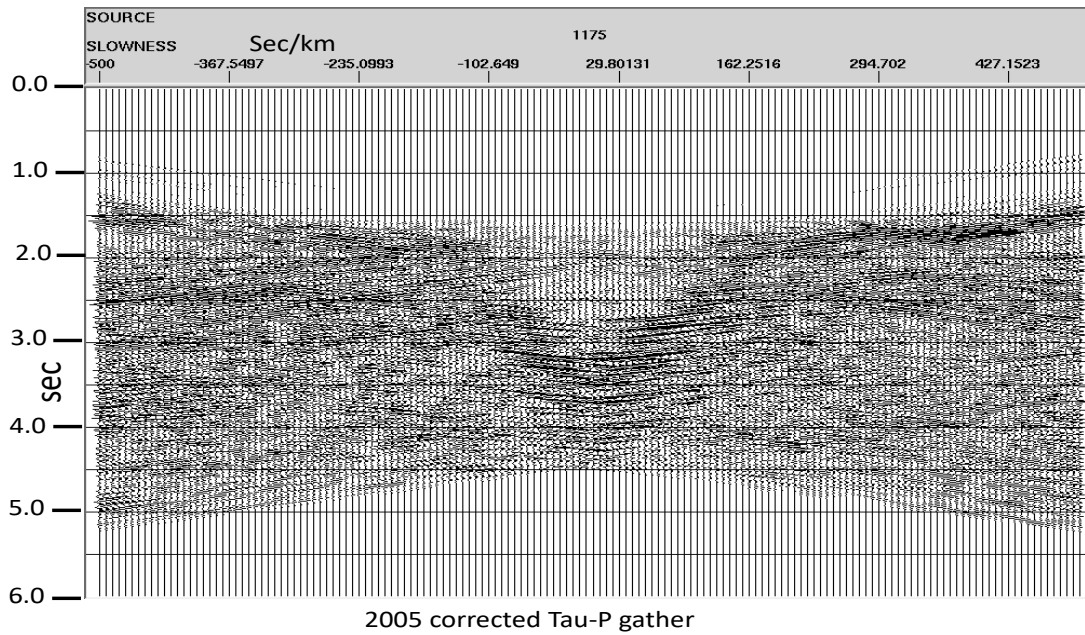


FIG. 32. Tau-P transform from Figure 26 with all surface functions for all ray parameters applied to remove near-surface effects.

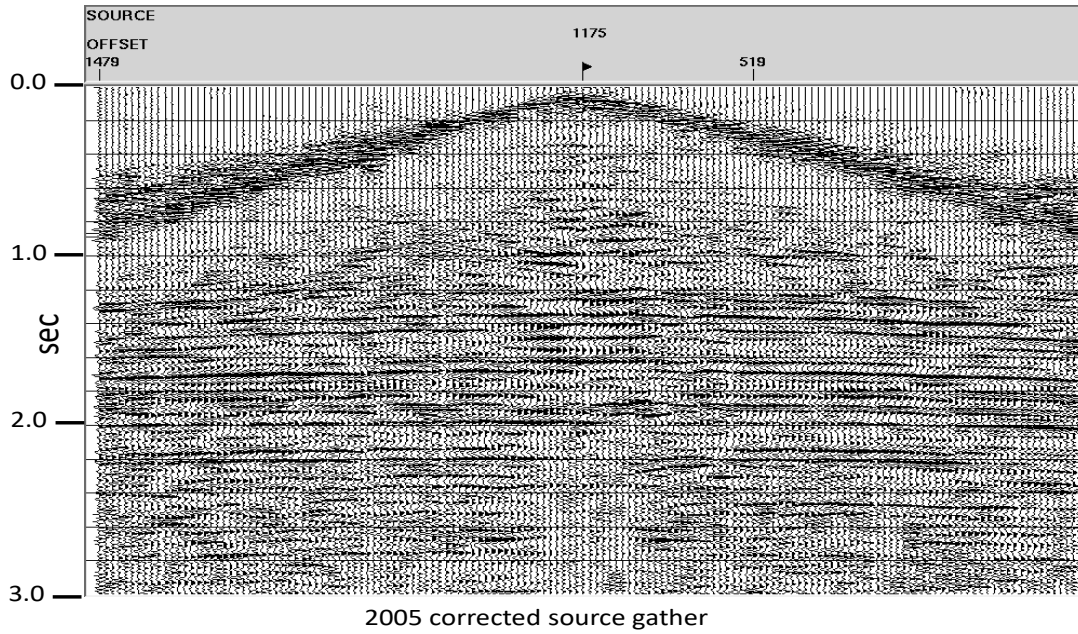


FIG. 33. Source gather from 2005 baseline survey after raypath interferometry, before application of initial muting.

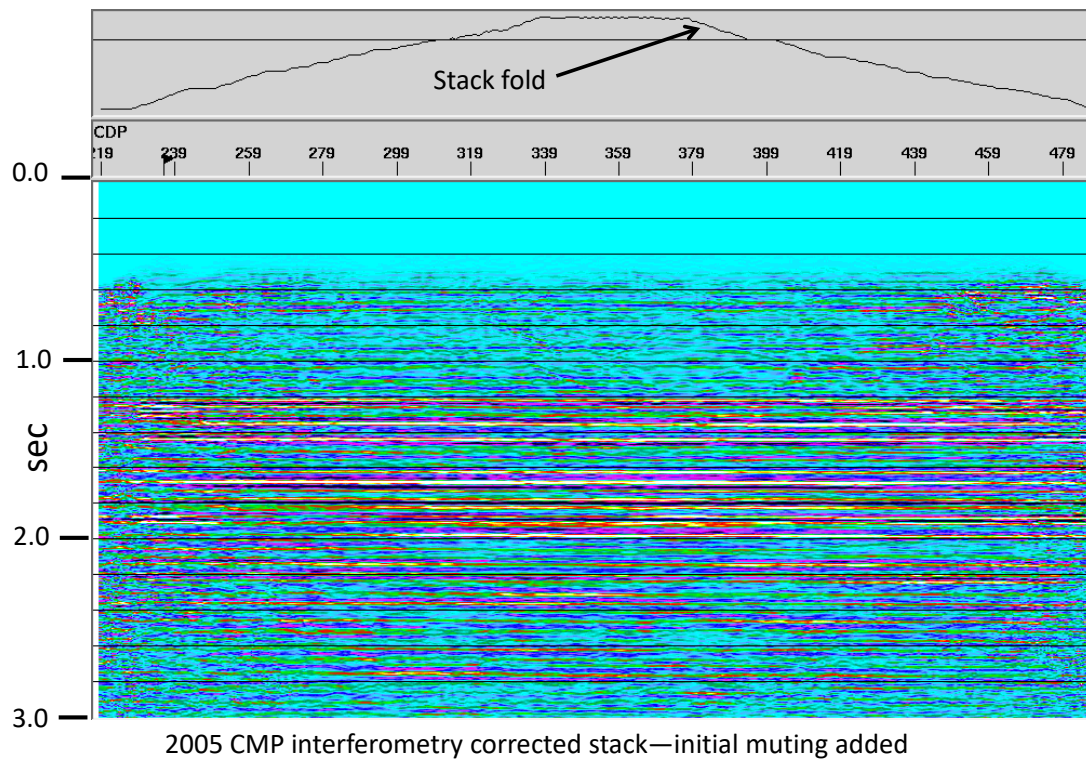


FIG. 34. CMP stack of 2005 source gathers after raypath interferometry and initial muting applied.

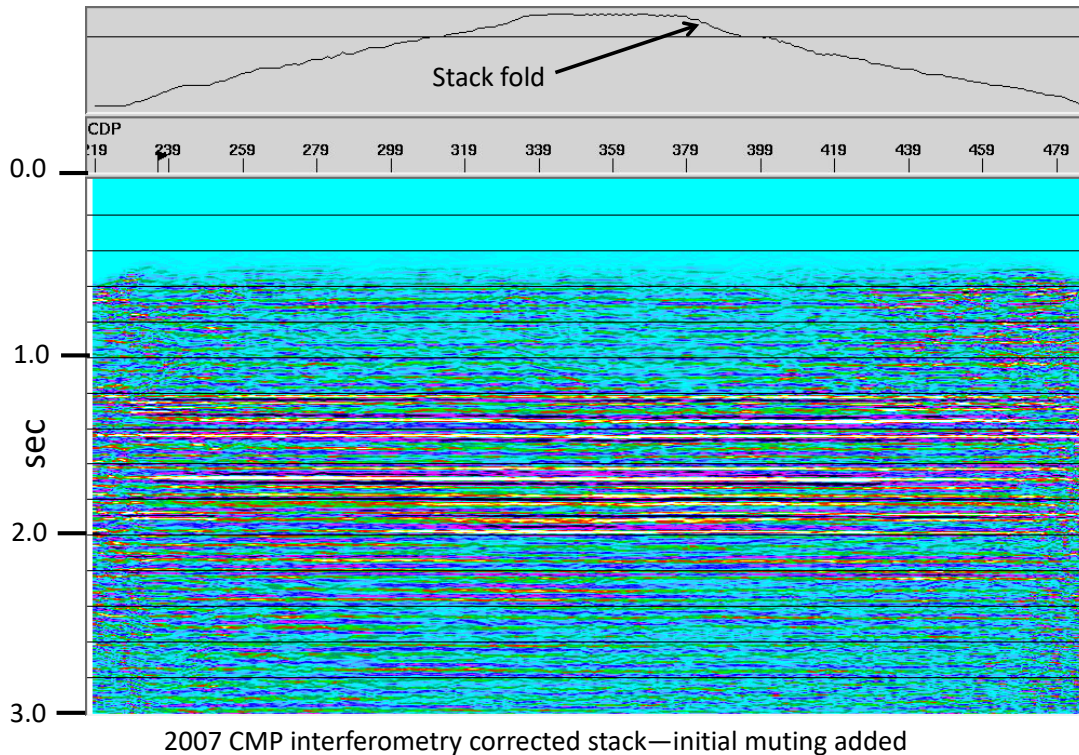


FIG. 35. CMP stack of 2007 source gathers after raypath interferometry and initial muting applied.

Comparing the surveys--details

Unlike more conventional time-lapse comparisons, where reflection amplitude anomalies are the key indicator of changes in rock properties induced by fluid injection, we seek reflection transit time anomalies. Since we hope to detect transit time differences as amplitude anomalies *caused by the subtraction of slightly misaligned reflection events*, we need to approach trace amplitudes in a different manner than we would if looking for simple reflection amplitude differences. To detect the latter, we would process both baseline and time-lapse data sets in such a way as to carefully preserve relative amplitudes of all reflection events, so that any residual amplitude from the subtraction of perfectly aligned events might be interpreted as an underlying change in reflectivity of a rock layer boundary. To detect only the *amplitude anomalies due to time shifts*, however, we must process the traces in such a way as to minimize the amplitude differences of any perfectly aligned events. One way to do this is to apply a trace equalization operation, in which the average (or rms) amplitude of a trace within a window is forced to be the same as the average or rms amplitude in the same window of the corresponding trace to be subtracted. Since the event sequence and waveform in the two trace segments should be the same for a time-lapse experiment, the event amplitudes after equalization should be similar enough between the two traces that actual residual amplitude differences after subtraction are quite small, unless corresponding events are misaligned, as we showed in our experiment in Figures 13-16.

When examining the CMP stack images of the baseline and time-lapse surveys, if a long-wavelength amplitude trend (with time) is observed on the traces, a long-window (700ms) AGC can be applied to all CMP traces prior to trace equalization. Figure 36 shows gated portions of matched pairs of traces from the 2005 baseline and 2007 time-lapse surveys after AGC, but before trace equalization, while Figure 37 shows the same traces after equalization. Although there is little visible difference between these figures, if we display the actual trace differences, as in Figures 38 and 39, we find that the overall trace differences are lower in amplitude after trace equalization, as we expect. More importantly, however, we observe that *relative* event amplitudes on the difference traces after trace equalization have changed. For example, in Figure 39, event differences above 1200ms remain nearly unchanged after normalization, while those beneath 1200ms are larger in amplitude. We maintain that since the trace equalization minimizes actual amplitude differences between the two vintages of traces, the amplitude residuals that we see are largely due to slight time mismatches between corresponding traces.

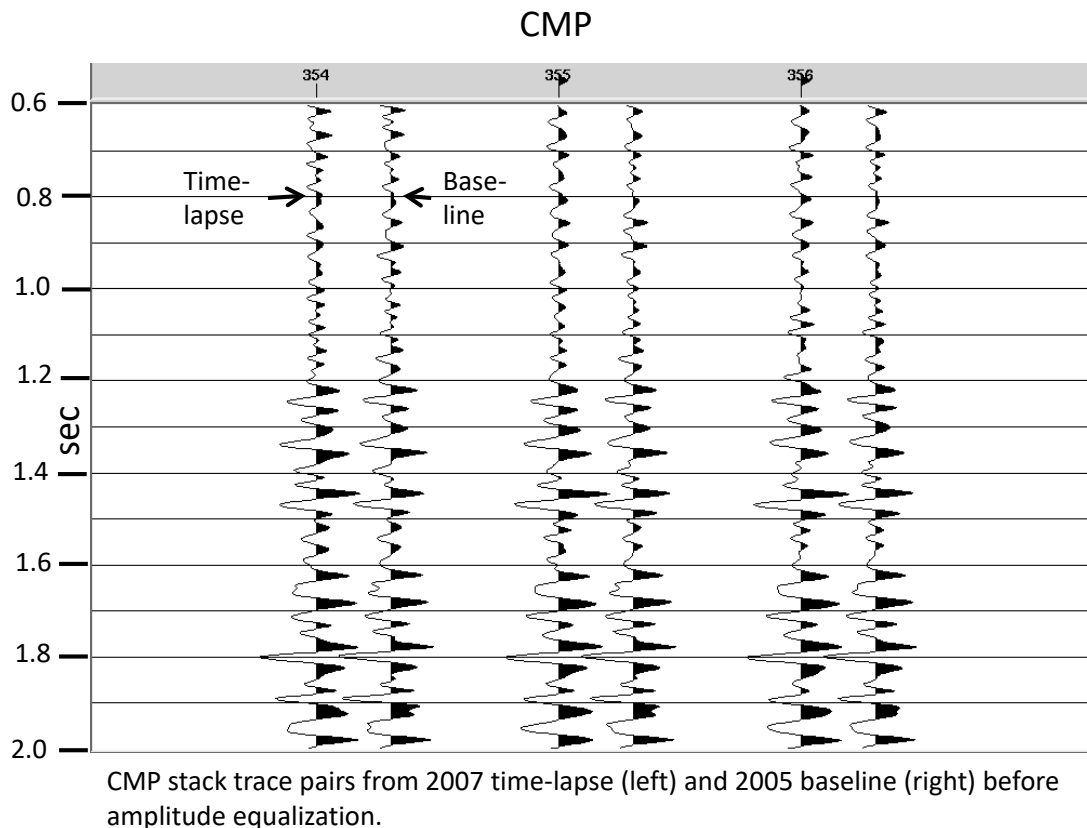


FIG. 36. Matched pairs of CMP stack trace segments before amplitude equalization based on average amplitude in a window. In each pair, the left trace corresponds to the 2007 time-lapse survey, and the right trace to the 2005 baseline survey.

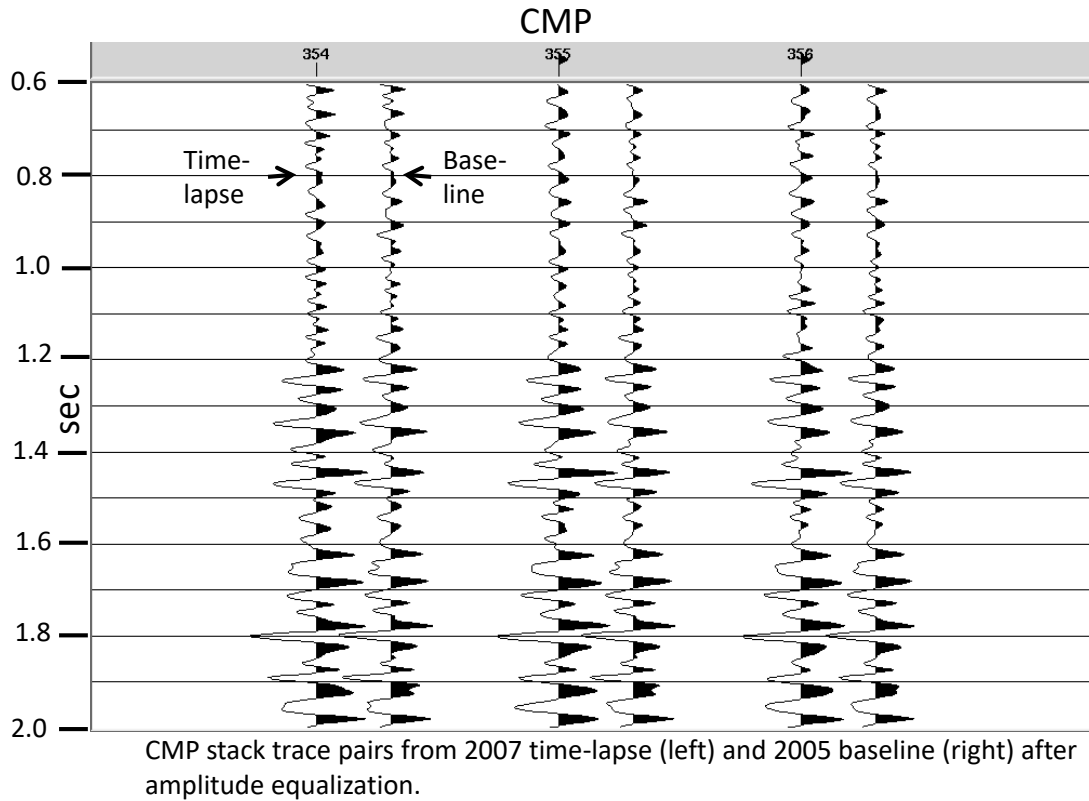


FIG. 37. Matched pairs of CMP stack trace segments after amplitude equalization based on average amplitude in a window. In each pair, the left trace corresponds to the 2007 time-lapse survey, and the right trace to the 2005 baseline survey. Visually, there is almost nothing to distinguish this figure from Figure 36.

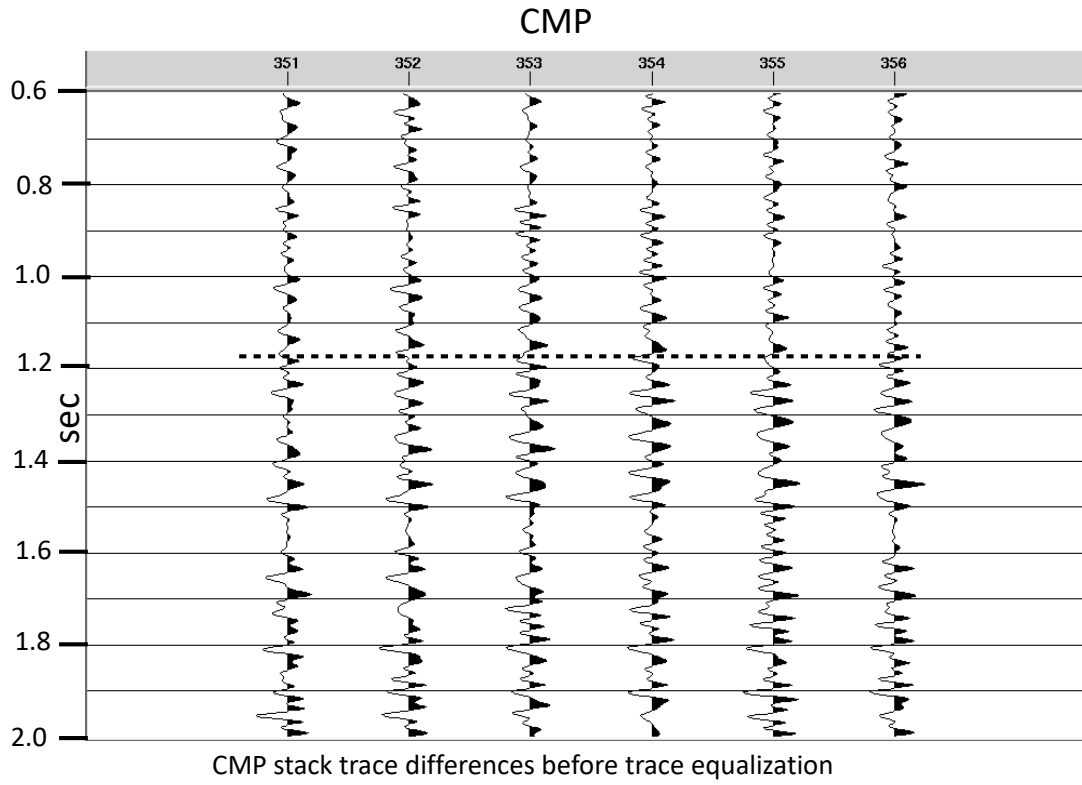


FIG. 38. Subtractive differences between the 2007 time-lapse CMP traces and the 2005 baseline CMP traces before trace amplitude equalization.

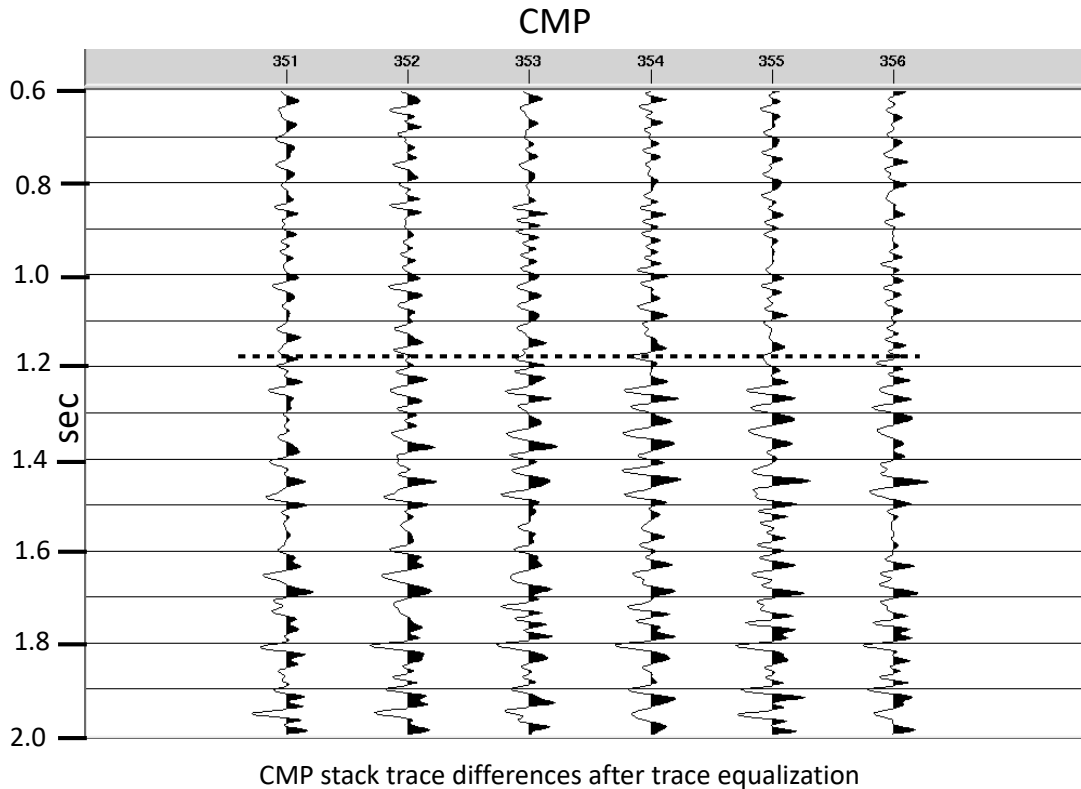


FIG. 39. Subtractive differences between the 2007 time-lapse CMP traces and the 2005 baseline CMP traces after amplitude normalization. The differences above 1200ms are virtually the same after normalization as before (Figure 38), while the deeper differences, below 1200ms are of larger amplitude. This implies that at least part of the deeper amplitude differences are due not to differences in amplitude on the two surveys, per se, but to slight timing mismatch of events.

RESULTS

The CMP stack of the 2005 baseline survey is shown in Figure 40, while the CMP stack of the 2007 Violet Grove time-lapse survey is displayed in Figure 41. Comparing the two displays visually gives no hint as to the expected anomaly due to CO₂ injection. When the two sections are normalized (trace equalization) and subtracted as described above, the difference image is as shown in Figure 42. In this figure, the expected anomalous zone is roughly the yellow ellipse, whose upper boundary coincides with the location of the originally-expected reflection *amplitude anomaly*. The red dashed lines give some idea of the expected zone of influence on event transit times by a low velocity zone located at the position of the unseen reflection amplitude anomaly. The fan shape is due to the fact that deeper event reflections will be affected at greater lateral distance by seismic traces corresponding to long-offset, shallow angle raypaths. Against a background of generally random amplitudes, the pattern seen in Figure 42 is just what we would expect to see for events slightly mismatched in time due to delays caused by a zone of lower velocity at about 1000ms. To verify that the difference amplitudes are solely caused by the time differences, we used the logic of interferometry with the two images being compared. We applied a time shift of 1.6ms to the baseline image and

performed the difference operation again. The result is shown in Figure 43, where now, most of the amplitude anomaly lies outside of the assumed zone of injection influence, and the amplitudes within this zone have been significantly diminished. This is the same effect as the simulation we showed in Figures 13-16, and we assert that since event amplitudes have been carefully normalized, the amplitude anomalies we observe are due mostly to reflection event time delay caused the lower-velocity zone created by CO₂ injection into the Cardium formation. The anomaly observed in Figure 42 does not fit neatly within the expected fan, with some effect being observed considerably to the right. We have no independent information regarding the actual position and extent of the CO₂ plume in this experiment, however, and it is entirely plausible that it extends further to the right of the injection point than to the left (see Figure 44).

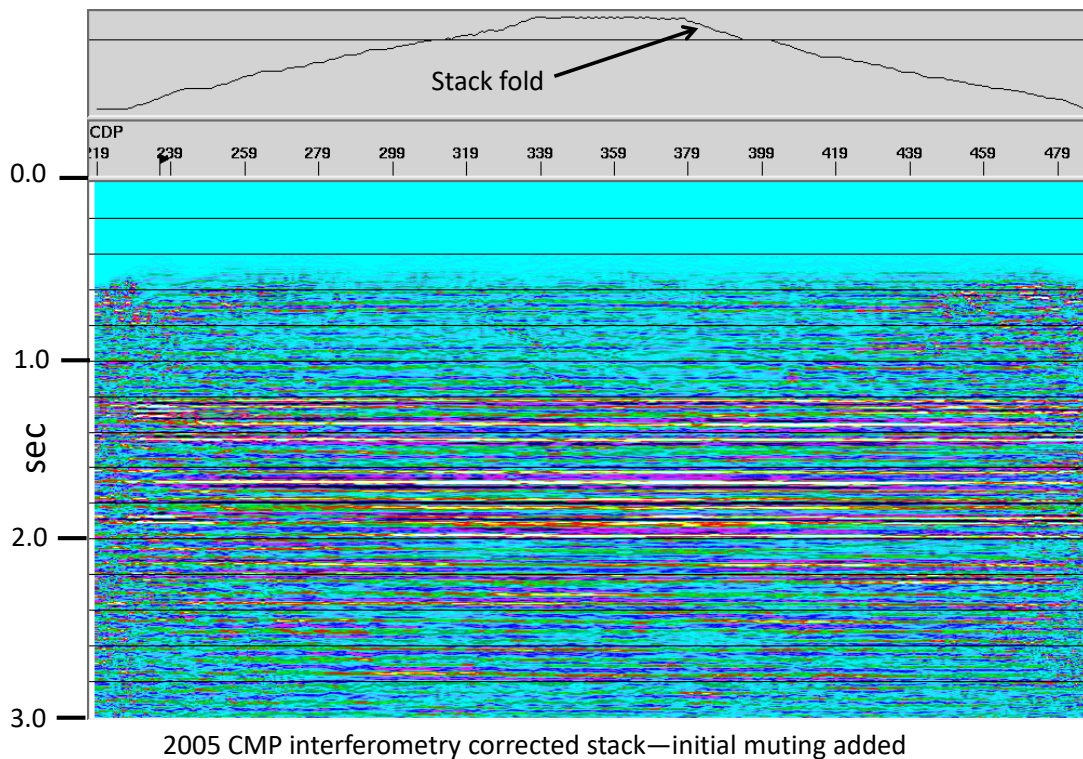


FIG 40. Final normalized CMP stack of the 2005 Violet Grove baseline survey.

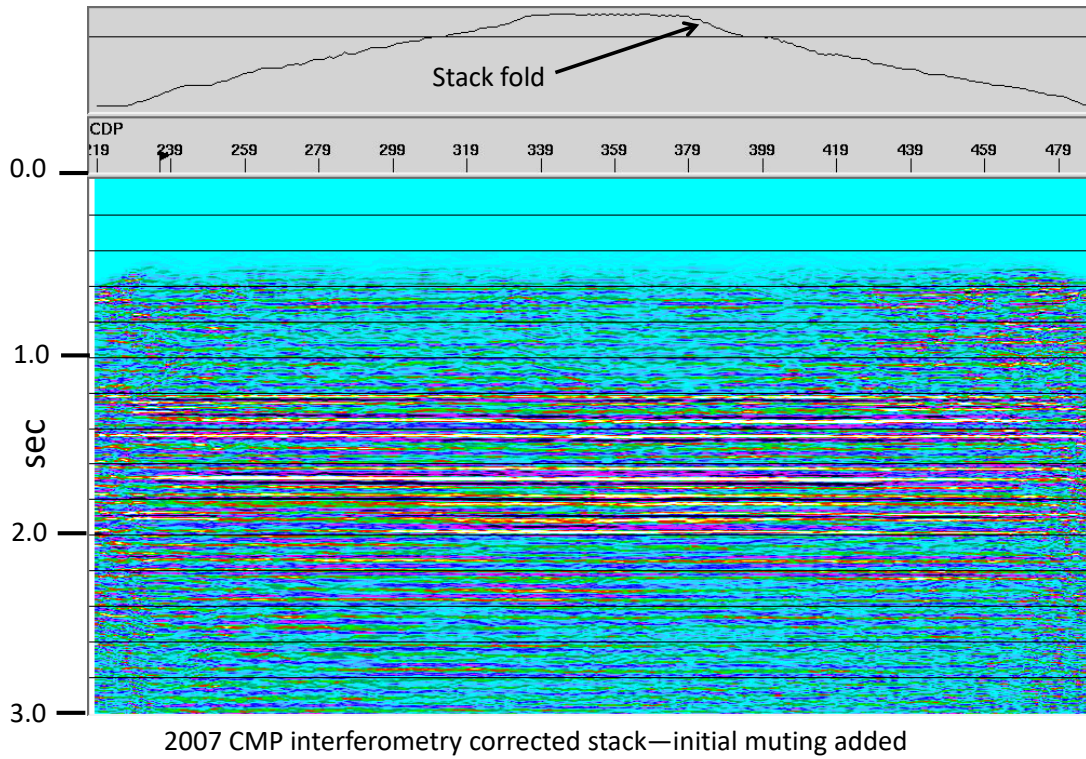


FIG. 41. Final normalized CMP stack of the 2007 Violet Grove time-lapse survey.

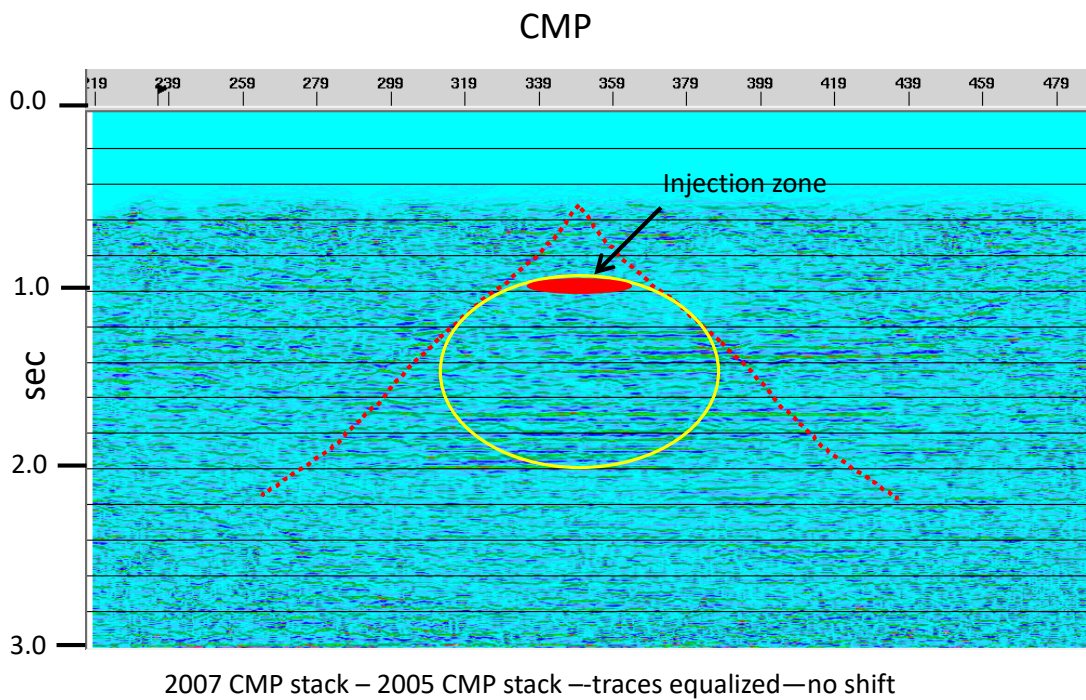


FIG. 42. Subtractive difference between the images in Figures 40 and 41. Yellow ellipse shows the main part of the time sag, red cone illustrates the lateral increase of the zone with depth.

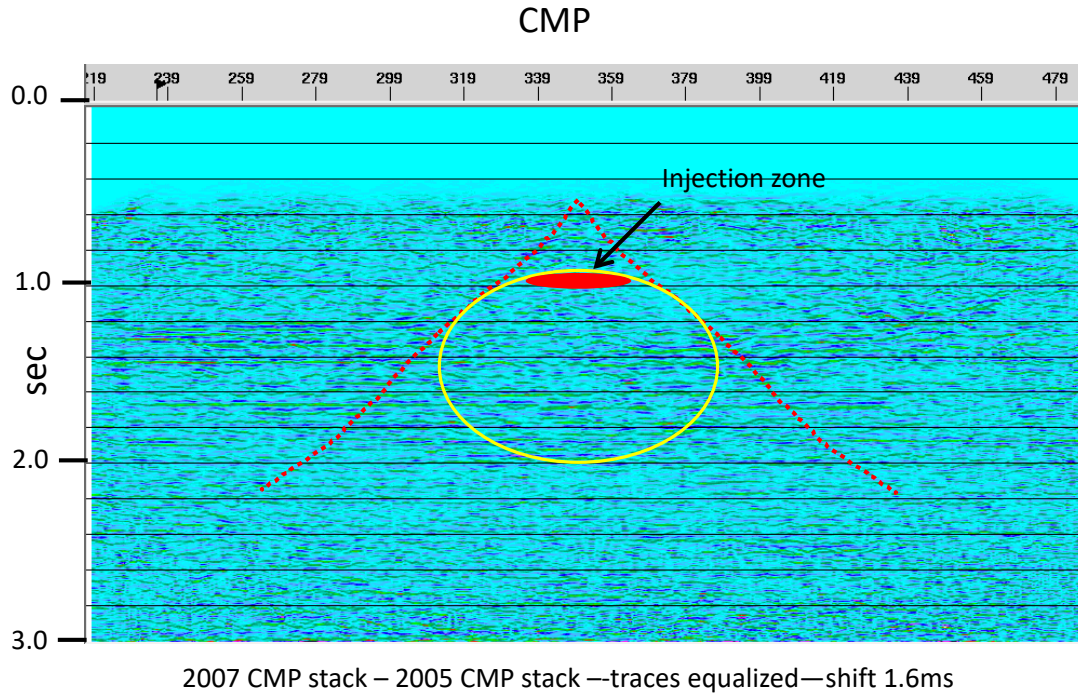


FIG. 43. Subtractive difference between the images of Figures 40 and 41 with Figure 40 shifted by 1.6ms. The amplitude anomalies due to event timing mismatch fade in the zone beneath the injection target zone but bloom toward the flanks, as we expect from modeling. Experimentation with different time shifts indicates that the actual time sag of reflection events beneath the expected Cardium anomaly is in the neighborhood of 1.6ms \pm 0.3ms.

As we experimented with these data, we found that relative time shifts of as little as 0.5ms were sufficient to cause visible changes in the time-sag anomaly position; we thus consider this method to be a potentially very sensitive tool for detecting the influence of fluid injection. The time shift which seemed to show the most contrast with the zero-shift case was 1.6ms, so we consider that this is a reasonable estimate for the average delay time added to reflections beneath the Cardium anomaly.

As an interesting speculation, if we displace the purported injection zone laterally, and enlarge it, as in Figure 44, we find that the time shift anomalies fit even better. We have moved the ellipse and cone accordingly. Is it possible that the injection fluid flowed asymmetrically from the borehole, given the well-known heterogeneity of the porosity distribution of the Cardium formation?

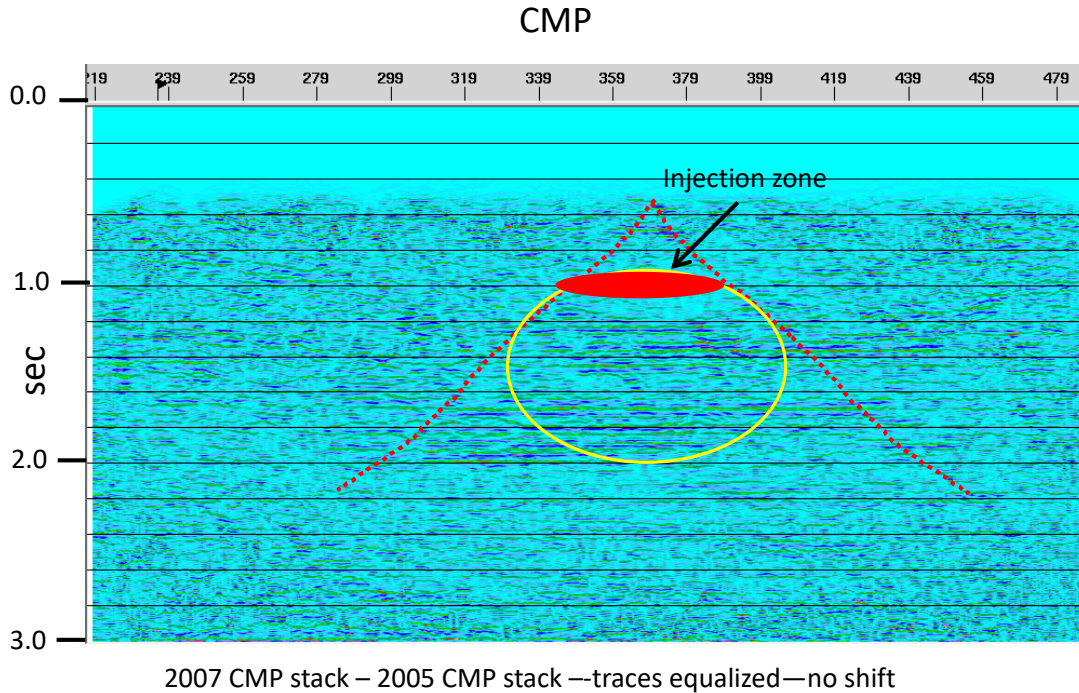


FIG. 44. If the fluid injection proceeded asymmetrically to the right from the borehole, the time-shift anomaly pattern fits even better than shown in Figure 42.

DISCUSSION/CONCLUSIONS

Thanks to some unexpected results on a time-lapse modeling study, which we described at the beginning, we hypothesized that in some cases, detecting the subtle travel-time delays induced in layers beneath a time-lapse target might be more feasible than detecting the small reflection amplitude changes at the target's upper and lower boundaries. We first tested the detectability of very small relative time shifts using a model based on a real field data survey, in which *only* the event transit times changed—the amplitudes were exactly the same. We showed that time delays as small as $\frac{1}{4}$ the sample interval were readily detectable, even with a very high level of bandlimited random noise added to the source gathers. Realizing from this experiment that properly registering the respective images of the baseline and time-lapse surveys was crucial, we used joint raypath interferometry to apply surface corrections to the two Violet Grove surveys, *using the same reference wavefield*, which automatically registers the images. We then removed, via initial muting, the residual coherent noise on all source gathers, as well as shallow reflection information. In order to minimize any image differences that might be due to actual reflection amplitude anomalies, we carefully equalized the amplitudes of all traces to be subtracted. After this equalization and the subsequent image subtraction, we found amplitude anomalies in several reflections beneath the CO₂ injection zone in the Cardium formation. The pattern of these anomalies, laterally expanding with depth, strongly suggests that we are observing primarily time delay anomalies in the reflections, the lateral spread being due to raypaths at longer offsets and deeper times. As a check on our hypothesis that the observed anomalies are due primarily to time shift, we found that we could greatly diminish the amplitude of the time-sag

anomalies by applying a small shift to the baseline survey before subtraction, and that this shift then led to the appearance of mismatch anomalies on the flanks of the originally observed anomaly. We note that the original time anomaly appears to be displaced to one side of the injection site. We speculate that one explanation of this would be an asymmetric fluid flow during injection, possibly due to the heterogeneity of the Cardium porosity distribution.

ACKNOWLEDGEMENTS

The author gratefully acknowledges financial support from the CREWES consortium, as well as NSERC. Helpful discussions with G. Margrave, K. Innanen, and D. Lawton are also acknowledged.

REFERENCES

- Almutlaq, M.H., and Margrave, G.F., 2010, Towards a surface-consistent match filter (SCMF) for time-lapse processing, CREWES Research Report Volume **22**(2010).
- Almutlaq, M.H., and Margrave, G.F., 2011, Application of a surface-consistent matching filters (SCMF) on a time-lapse dataset, CREWES Research Report Volume **23**(2011).
- Almutlaq, M.H., and Margrave, G.F., 2012a, Surface-consistent matching filters for time-lapse seismic processing, CREWES Research Report Volume **24**(2012).
- Almutlaq, M.H., and Margrave, G.F., 2012b, Violet Grove time-lapse data revisited: a surface-consistent matching filters application, CREWES Research Report Volume **24**(2012).
- Almutlaq, M.H., and Margrave, G.F., 2013, Surface-consistent matching filters for time-lapse seismic processing, *Geophysics* **78**, No. 5, ppM29-M41.
- Alshuhail, A., and Lawton, D.C., 2007, Time-lapse surface seismic monitoring of injected CO₂ at the Penn West CO₂-EOR site, Violet Grove, Alberta, CREWES Research Report Volume **19**(2007).
- Alshuhail, A., Lawton, D.C., and Chabot, L., 2008, Pembina Cardium CO₂ monitoring project: time-lapse seismic analysis, CREWES Research Report Volume **20**(2008).
- Chen, F., and Lawton, D.C., 2005, Interpretation of baseline surface seismic data at the Violet Grove CO₂ injection site, Alberta, CREWES Research Report Volume **17**(2005).
- Cova, R., Wei, X., and Innanen, K.A.H., 2015, Shear wave near-surface corrections in the tau-p domain: a case study, CREWES Research Report Volume **27**(2015).
- Henley, D.C., 2012a, Interferometric application of static corrections, *Geophysics*, **77**, No. 1, pp Q1-Q13.
- Henley, D.C., 2012b, Interference and the art of static correction: raypath interferometry at Hussar, CREWES Research Report Volume **24**(2012)
- Henley, D.C., Wong, J., and Manning, P.M., 2012, Time-lapse by the numbers: elastic modeling of repeatability issues, CREWES Research Report—Volume **24**(2012).
- Henley, D. C., Wong, J., and Manning, P.M., 2016, Time lapse survey repeatability: an elastic modeling study, *CSEG Recorder*—Volume **41**, No. 9 (December 2016), pp 36-39.
- Lawton, D.C., Coueslan, M., Chen, F., Bland, H.C., Jones, M., Gallant, E., and Bertram, M., 2005, Overview of the Violet Grove CO₂ seismic monitoring project, CREWES Research Report Volume **17**(2005).
- Liu, Y., Lawton, D.C., and Margrave, G.F., 2005, Well-seismic bandwidth and time-lapse seismic characterization: physical considerations, CREWES Research Report Volume **17**(2005).
- Liu, Y., and Lawton, D.C., 2006, Well-seismic bandwidth and time-lapse seismic characterization related to CO₂ injection and fluid substitution: physical considerations, CREWES Research Report Volume **18**(2006)
- Lu, H., Hall, K.W., and Lawton, D.C., 2005, Violet Grove 2D and 3D data processing at CREWES, CREWES Research Report Volume **17**(2005)
- Lu, H., Hall, K.W., and Lawton, D.C., 2006, Violet Grove 2D processing at CREWES update, CREWES Research Report Volume **18**(2006).
- Zhang, J.J., Bentley, L.R., Settari, T., and Krebs, E., 2005, Time-lapse seismic modeling in Leming Lake, Alberta, CREWES Research Report Volume **17**(2005).